Compact, High-g, Efficient Folding Wing for a Cannon-Launched Reconnaissance Vehicle

by

Thierry D. Casiez

B.Eng. Mechanical Engineering
McGill University, 1997

Submitted to the Department of Aeronautics and Astronautics in Partial Fulfillment of the Requirements for the Degree of Master of Engineering in Aeronautics and Astronautics

at the

Massachusetts Institute of Technology

June 1998

Author .....
Department of Aeronautics and Astronautics
May 8, 1998

Certified by .....
Charles Boppe
Senior Lecturer, Department of Aeronautics and Astronautics
Thesis Supervisor

Certified by .....
Carlos E.S. Cesnik
Boeing Assistant Professor of Aeronautics and Astronautics
Thesis Supervisor

Certified by .....
Mark Drela
Associate Professor of Aeronautics and Astronautics
Thesis Supervisor

Accepted by .....
Jaime Peraire
Chairman, departmental Graduate Committee

Compact, High-g, Efficient Folding Wing
for a Cannon-Launched Reconnaissance Vehicle

by

Thierry D. Casiez

Submitted to the Department of Aeronautics and Astronautics
on May 8, 1998, in partial fulfillment of the requirements for the degree of
Master of Engineering in Aeronautics and Astronautics

Abstract

The Cannon-launched Reconnaissance Vehicle (also known as WASP or Wide Area Surveillance Projectile) was developed within the context of the MIT / Draper Technology Development Partnership Project. The development objective was a first-of-a-kind system within a time frame of two years and the development of an entrepreneurial spirit among the involved engineering students at MIT. The final concept consisted of an integrated shell-flyer system. After being launched from a standard Navy gun, the shell would immediately deploy fins for the fin-stabilized ballistic phase. Then a parachute would deploy to extract the flyer from the shell. At this point the flyer would be ready to deploy aerodynamic surfaces (wings and tails), and would conduct a 15-minute surveillance mission, recording images with a visual sensor, and sending them back to a ground station.

This report shows the design of a compact, high-g, efficient folding wing as part of the overall system design effort. It addresses the structural wing design for both the high-g and the flight conditions, as well as the aerodynamic design for the wings and the static stability design for the overall flyer. The design work was achieved using existing analytical software tools and field gun testing, the latter also permitting the ultimate validation of the design.

Thesis Supervisor: Charles Boppe
Title: Senior Lecturer, Department of Aeronautics and Astronautics

Thesis Supervisor: Carlos E.S. Cesnik
Title: Boeing Assistant Professor of Aeronautics and Astronautics

Thesis Supervisor: Mark Drela
Title: Associate Professor of Aeronautics and Astronautics

Acknowledgments

I would like to thank the MIT / Draper project team for their support, enthusiasm, and for a very great year, including Mr. Charles Boppe and Professor John Deyst. Special thanks to Professor Carlos Cesnik, Professor Mark Spearing and Professor Mark Drela for their enthusiasm, guidance and support.

I would also like to thank the Charles Stark Draper Laboratory for giving me the chance to participate in such an exciting venture.

Special thanks to Dr. Brent Appleby, who provided very appreciated support and enthusiasm to the project, in his functions of student liaison between MIT and the Draper Laboratory. Special thanks also to Mr. John Mahoney who machined many of the flyer metal parts and who was very dedicated to the project and provided us with top quality hardware. Thanks to Greg Kirchos, engineer at the Draper Laboratory, who performed some Finite Element Analyses for the wing design.

I would like to thank my family for their support through this year. "Merci a Papa et Maman pour m'avoir donne la chance d'arriver jusqu'ici, merci pour votre support, et merci aussi a mes freres et soeurs, Stanislas et Valerie, pour votre support."

"Merci Rana pour m'avoir donne support et tendresse, qui m'ont aussi aide a aller jusqu'au bout."

Table of Contents

List of Figures

PAGE

List of Tables

PAGE

Symbols

A	wing area (excluding fuselage)
AR	aspect ratio
C_D	drag coefficient
C_{Di}	induced drag
CG	center-of-gravity
C_L	lift coefficient
Clα	lift curve slope
Clβ	rolling moment coefficient derivative due to sideslip
Clp	rolling moment coefficient due to roll rate derivative
Clq	rolling moment coefficient due to pitch rate q
Clr	rolling moment coefficient due to yaw rate derivative
Cmα	pitch stiffness
Cmq	pitch damping derivative
Cnβ	yawing moment coefficient due to sideslip derivative
Cnp	yawing moment coefficient due to roll rate derivative
Cnr	yawing moment coefficient due to yaw rate derivative
CYβ	side force coefficient due to sideslip derivative
CYp	side force coefficient due to roll rate derivative
CYr	side force coefficient due to yaw rate derivative
D	drag force
e	Oswald efficiency factor
e_p	propeller efficiency
g	gravitational constant
L	lift force
m	flyer mass
P	engine power
ρ	air density
T	thrust force
V	flight velocity
W	flyer weight

Chapter 1 Introduction

1.1 The MIT/Draper Technology Development Partnership Project

In 1996, The Charles Stark Draper Laboratory approached the Massachusetts Institute of Technology to create a technology Development Partnership Project. This project constituted an attempt to establish a partnership with the two parties that would result in the development of a first-of-a-kind nationally important product. The Partnership Process Elements and Relationships are defined on Figures 1(A) and 1(B).

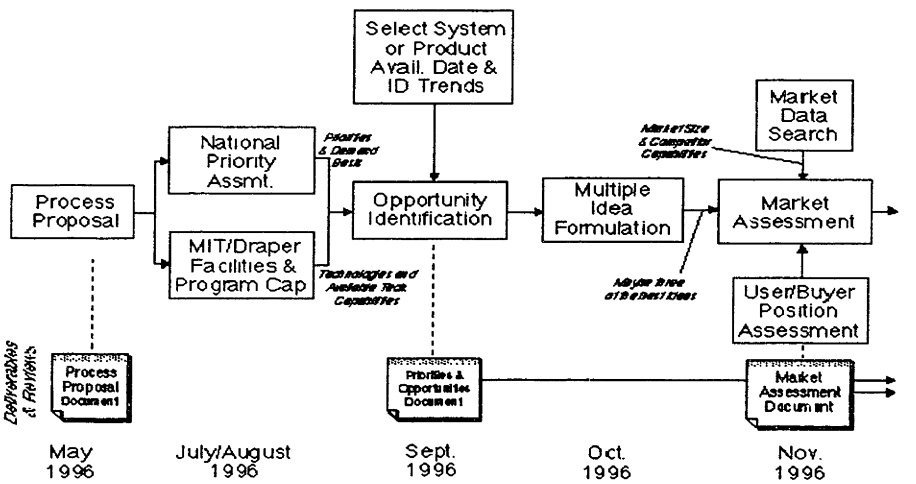

FIGURE 1(A): PARTNERSHIP PROCESS ELEMENTS AND RELATIONSHIPS

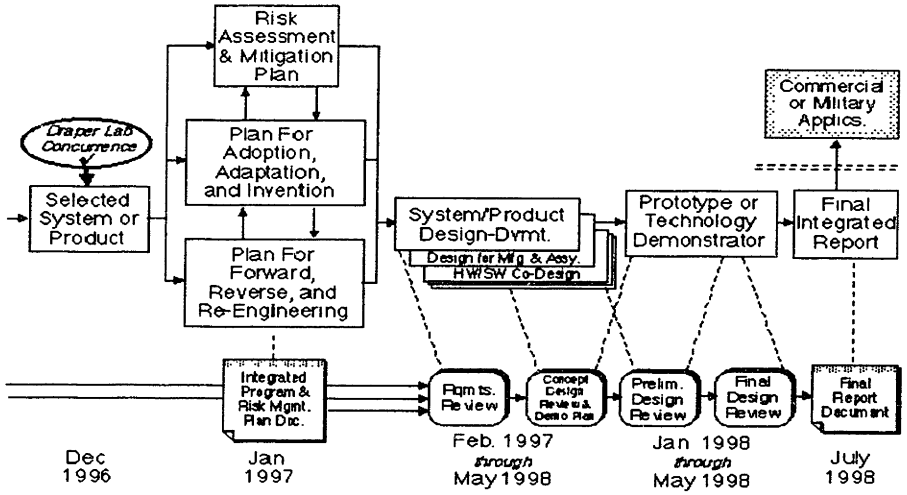

FIGURE 1(B): PARTNERSHIP PROCESS ELEMENTS AND RELATIONSHIPS

1.2 The Wide Area Surveillance Projectile (WASP)

The goals of the technology development partnership project were the following:

- Concept to hardware/software demonstration in two years
- Innovations and creativity
- Development of an entrepreneurial spirit among the involved engineering students
- Multi-disciplined concept
- Take full advantage of the Draper Laboratory and MIT capabilities
- A first-of-a-kind, nationally important system / product
- High risk... "unobtainium"

An intensive study was conducted in the first year of the project to find the most suitable candidate that would achieve the above-mentioned goals. The chosen concept was a cannon-launched reconnaissance vehicle (also known as WASP or Wide Area Surveillance Projectile).

The WASP has a specific target market defined by its mission niche, illustrated by Figure 2. As a wide area surveillance means, the WASP offers two main key elements: the fastest response time and control at a lower level of command since it is relatively inexpensive. The

WASP definitely offers the fastest response time of the other surveillance means because of its gun-launched capability.

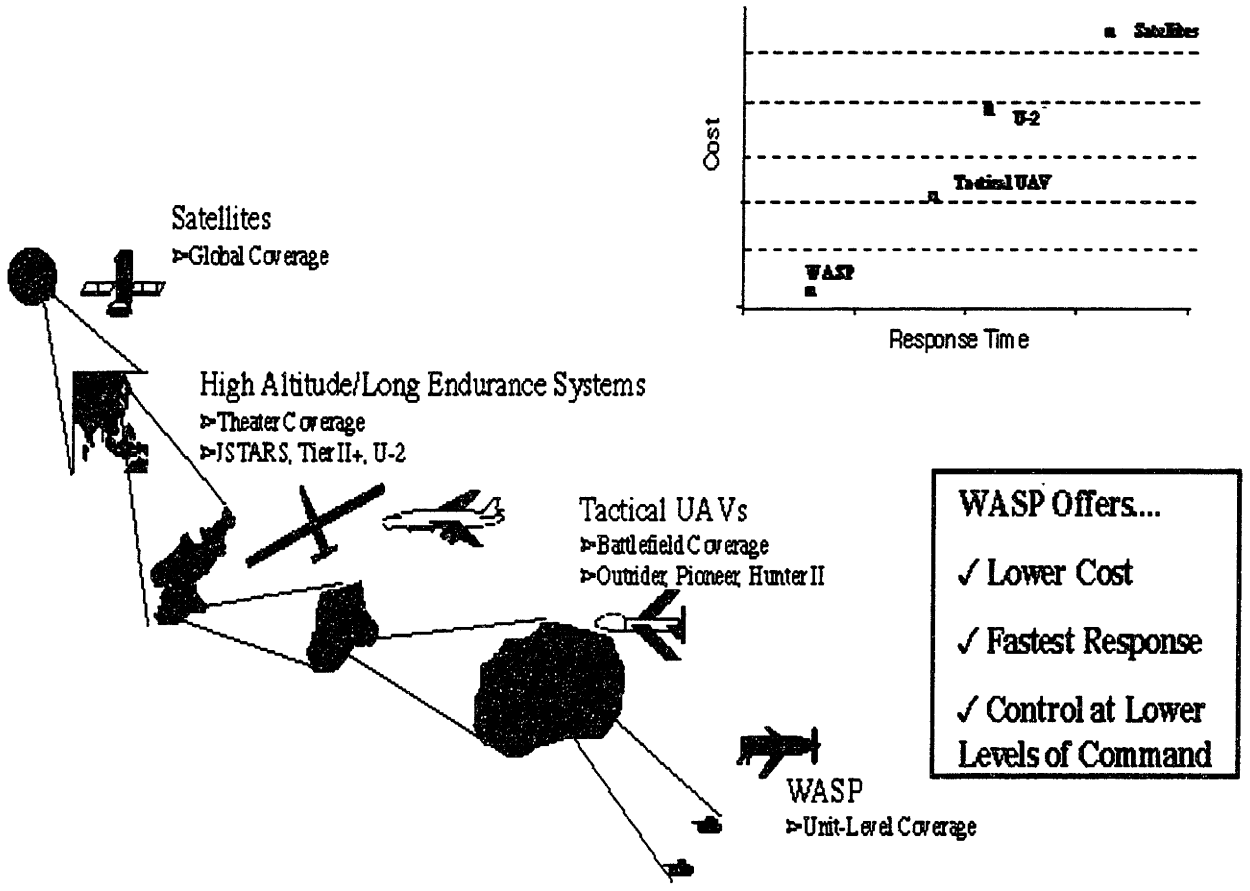

FIGURE 2: MISSION NICHE

A concept scenario for the WASP is illustrated on Figure 3, where the WASP could be used to support a precision guided munition mission. Such a precision guided munition is currently being developed by Draper as an Advanced Technology Development (ATD) program.

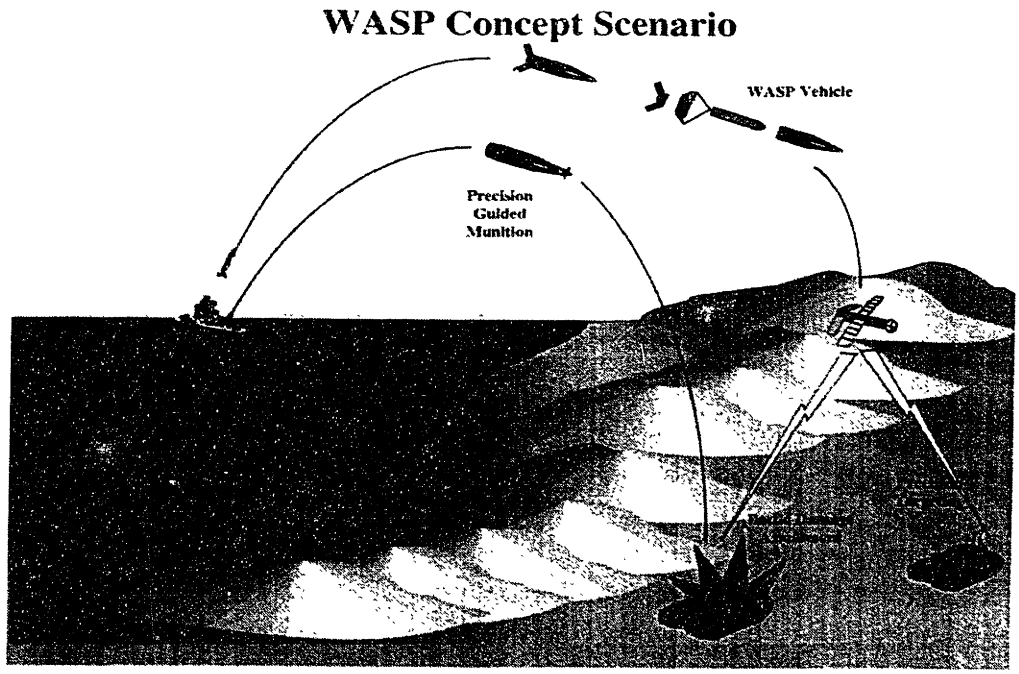

FIGURE 3: CONCEPT SCENARIO

1.3 The Team

The Department of Aeronautics and Astronautics provided most of the MIT team participants. These include nine graduate students, five Master of Engineering students (Sebastien Katch, Jean-Marc Hauss, Rodney Chiu, Garret Shook, and the author), and four Master of Science students (Vladislav Gavrilets, Staci Jenkins, Torrey Radcliffe, and Tan Trinh), as well as one undergraduate student (Padraig Moloney). MIT professors complete the MIT team, these are the project advisors (Charles Boppe and John Deyst) and the student advisors (Carlos Cesnik, Mark Spearing, Mark Drela, James Kuchar, and Peter Young).

From the Draper Laboratory, the student liaison between MIT and Draper is Brent Appleby. Engineers and machinists were also involved in the project.

This report addresses the accomplishments of the second year of the project, which has the following goals:

- Final concept refinement
- Detailed design
- Manufacturing, assembly, and test

and in particular, it will focus on the wing subsystem design.

Chapter 2 Cannon-Launched Reconnaissance System

2.1 Requirements

Once the concept was chosen to be a cannon-launched reconnaissance vehicle, requirements were generated for its design. These are summarized below:

- Compatible with a 5-inch Navy gun
- Survive launch forces, including a 15,000 g set back, 4,000 g set forward, and 1,000 g centrifugal accelerations
- Loiter for 15 minutes
- Autonomous operation with sensor
- Inexpensive, storable
- Ground station to receive real-time images and GPS coordinates of targets

2.2 Mission

These requirements led to a mission sequence definition. Figure 4 illustrates the mission deployment sequence, from gun launch to image transmission.

The sequence of events is as follows: the shell is loaded into a 5-inch gun such as the ones on a Navy ship. Then it is fired and as soon as it exits the barrel, six fins deploy which provide a stable ballistic flight. After an 11 nautical miles ballistic trajectory, while still at altitude, a parachute pulls a stowed aircraft from the back of the shell. The parachute is then jettisoned and the flyer is now free and deploys tails and propeller, and the engine starts. After approximately twelve seconds of parachute deceleration, the wings deploy and the parachute and ballistic stabilizing fins are released, leaving the flyer in its final mission configuration. The flyer then loiters and sends images to the ground station for fifteen minutes. This includes approximately ten minutes of powered flight and the remaining time of gliding flight.

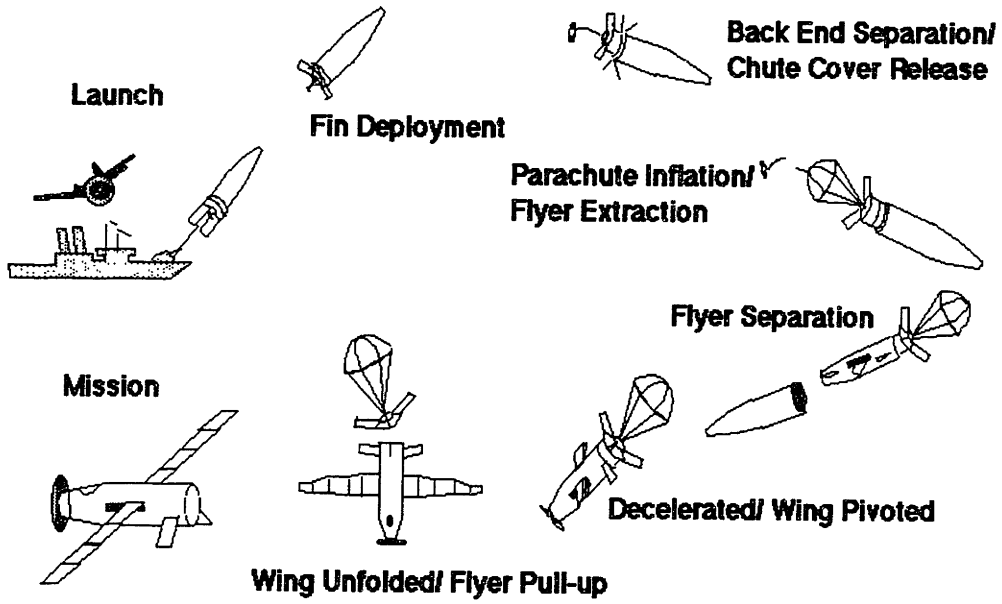

FIGURE 4: MISSION DEPLOYMENT SEQUENCE

2.3 Concept Demonstration

In order to demonstrate the operational vehicle concept, the decision was taken to design two vehicles (see Figure 5). The first vehicle, the High-G Vehicle (HGV) would be launched from a 5-inch gun and would include all necessary mechanical hardware to carry the mission up to and including the deployed flyer, ready to transmit live images. Then the mission would be carried on by the second vehicle, the Flight Test Vehicle (FTV), which would be a geometrically scaled up version of the HGV. The FTV would include off-the-shelf sensors and necessary electronics to transmit live images to the ground station and to perform autonomous stable flight, thus validating the flight characteristics of the HGV. The reason for developing the FTV is explained in section 2.4.

With both vehicles, the overall operational vehicle concept would be demonstrated, by linking the capabilities of the HGV to those of the FTV.

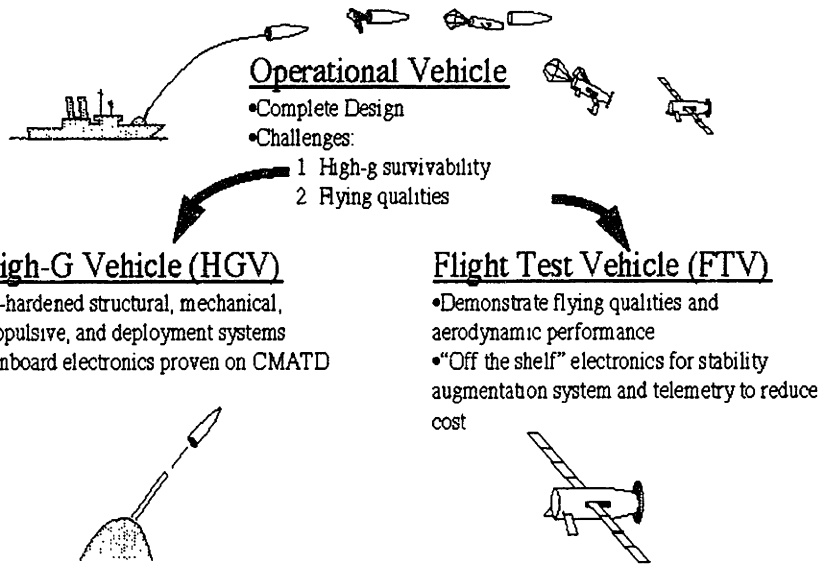

FIGURE 5: CONCEPT DEMONSTRATION

2.4 Top-Level Architecture

The design concepts, for the operational vehicle, the high-g vehicle, and the flight test vehicle, are presented below.

2.4.1 Operational Vehicle

To fulfill the mission requirements, the operational vehicle was chosen to be a shell-flyer concept [5]. The concept is illustrated on Figure 4.

2.4.1.1 Shell

In order to achieve the transition from the ballistic phase to the flight mission phase, the concept of a flyer extracting itself from a protective shell was selected. The shell would protect the flyer from the harsh gun environment that includes high temperatures. The shell would also restrain the flyer from tearing itself apart due to the high-g rebound and balloting loads. The other

important reason for using a shell is that it adds considerable weight to the whole system, thus enabling a longer ballistic range. It also lowers the gun-launch g loads.

The extraction of the flyer from the shell occurs at the end of the ballistic phase and the extraction mechanism was chosen to be similar to an existing concept used by the standard Navy fleet-issue 5-inch illuminating round (see Figure 6). There the payload is extracted from the base of the shell with the help of an explosive charge located in the shell. This technology is already in use and proven, thus acting in favor of adapting it to the reconnaissance vehicle. The decision was then to adapt a 5-inch illuminating round shell in which the flyer would be inserted. Extraction would be affected by a parachute at the base of the flyer which would pull the flyer out of the shell, rather than an explosive charge located at the nose of the flyer. This concept is used in the illuminating round but would not be preferred here because the nose of the flyer is expected to be too fragile, with the folding propeller, its mechanism, and other delicate parts. A last major difference between the reconnaissance vehicle shell and the illuminating round shell is that the former is fin-stabilized whereas the other is spin-stabilized. Spin stabilization would have required a very precise mass distribution around the longitudinal shell axis, which was considered very difficult to achieve, due to the number of intricate parts and mechanisms inside the flyer. What's more, the de-spin action would be difficult to stop. Even though the fin-stabilization concept was selected, it still has drawbacks:

- Added drag from fins resulting in a shorter ballistic range.
- Increased mechanical complexity
- Length exceeding single ram capability
- Higher cost
- Increased storage volume

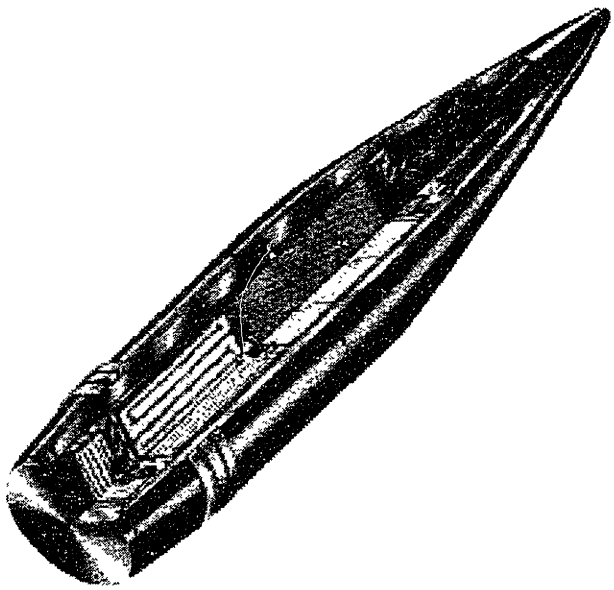

FIGURE 6: STANDARD NAVY FLEET-ISSUE 5"

2.4.1.2 Flyer

The flyer contained in the shell during the ballistic phase would be extracted and then ready to fly. In order to achieve its mission, a number of elements must be incorporated, namely a propulsion unit, some lifting surfaces, some control surfaces, a camera, and so on.

To group these elements together, and for ease of system manufacturing and assembly, the high-g vehicle was developed to be a modular design. This modularity concept is illustrated on Figure 7. Three modules constitute the flyer. These are the propulsion module, the wing module, and the tail module. Each of these modules incorporates a defined set of subsystems, detailed in Chapter 7.

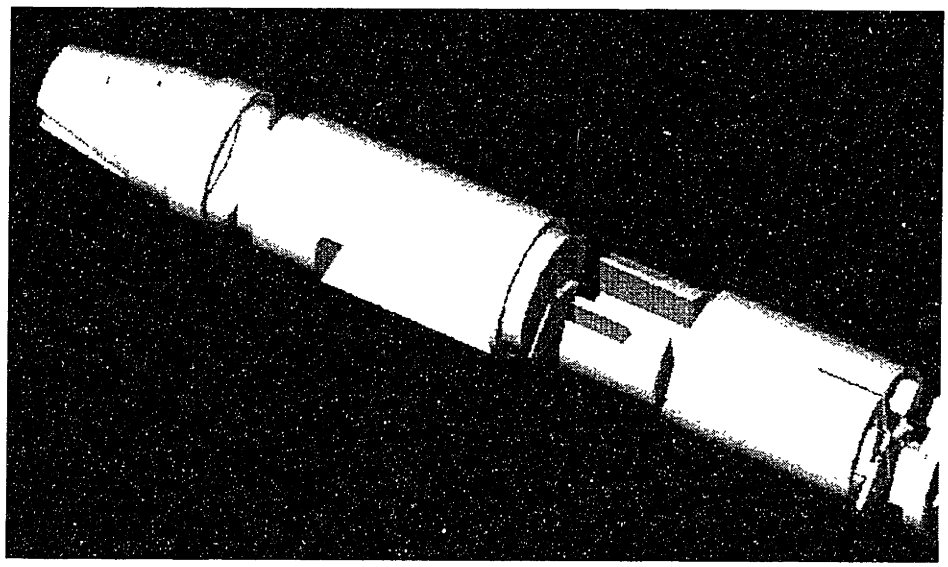

FIGURE 7: EXPLODED VIEW OF THE THREE FLYER MODULES

2.4.2 High-g Vehicle

The high-g vehicle was defined to be the operational vehicle without electronic equipment on board, for reasons explained in section 2.4.3.

2.4.3 Flight Test Vehicle

The reason for developing the FTV is that the electronic components needed to equip a fully operational vehicle would not be ready by the time of project completion. These special miniature high-g electronic components were mainly under development at the Draper Laboratory and their expected completion date was beyond the project end date.

Selected off-the-shelf electronic components to be inserted in the Flight Test Vehicle were found to be too large. The vehicle had to be geometrically scaled up by a factor of 1.28 with respect to the HGV dimensions. It did not feature any deployable elements since the on-board electronic components took up most of the space.

The goal of the FTV is to demonstrate handling qualities and aerodynamic performance, and sensor performance. Figure 8(A) shows the FTV with its on-board equipments in side view, and Figure 8(B) shows a front view of the vehicle

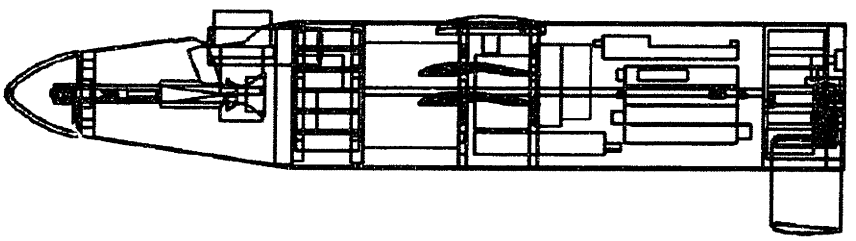

FIGURE 8(A): FLIGHT TEST VEHICLE: SIDE VIEW

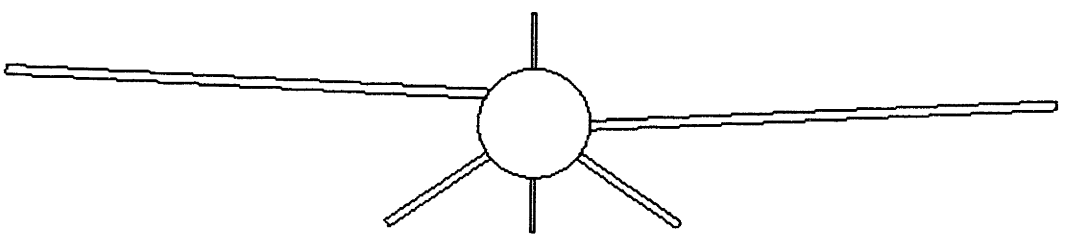

FIGURE 8(B): FLIGHT TEST VEHICLE: FRONT VIEW

2.5 Project Management

The modularity of the design created natural tasks assignments. Team members were divided into sub-teams, each responsible for the design of one of the modules of the flyer and its subsystems. Staci Jenkins and the author constituted the wing team.

Weekly meetings were conducted, including students, faculty and the MIT / Draper student liaison. These meetings assessed current status and important project decisions. Most of the meetings included a "featured speaker" to assess a design issue of the HGV or the FTV.

A schedule was carried through the year, with an attempt to update it regularly. The schedule was designed to give a global view of the project and to emphasize critical tasks leading to important deadlines. An example of a typical schedule is shown in Appendix A.

Chapter 3 Wing Development Concept Generation

3.1 Aerodynamic Configuration

3.1.1 flyer Preliminary Geometry

The fuselage shape is composed of a cone section in the front of the flyer plus a 3.9-inch diameter cylindrical section (internal diameter of the illuminating round shell), with a flat base. The cone length would span approximately a third of the total fuselage length, this latter being limited by the illuminating round shell to approximately 20 inches.

The engine-propeller, wings and tail locations on the flyer were mainly governed by the high-g loading the configuration has to sustain. More fragile folding propeller and cone components were placed in the front of the flyer where they would basically have to support only their own weight. The cut through the flyer structure needed for deploying the wings would be larger than the one needed for deploying the tails. In the aft region of the flyer, a smaller cut is desirable for structural reasons, therefore it was decided that the tails be positioned at the back, while the wings would lay between the propulsion unit and the tails. This resulted in a conventional airplane geometry.

3.1.2 Lifting Surfaces

In the early design phases, some brainstorming was done to come up with different lifting surfaces. A parasail wing emerged as a suggestion for the flyer. The very light weight of the cloth-type parasail appeared attractive for the high-g environment. However the aerodynamic characteristics of such lifting surface are not attractive. In fact, parasail vehicles have glide ratios much smaller than that of a standard fixed wing vehicle. The decision was then made to investigate the possibility of better performance wing designs.

3.2 Deployment Concepts

3.2.1 Telescopic Wings

The first wing deployment concept originated from the observation of telescopically-deployable objects, e.g., deployable fishing rod, automobile antennas, etc. This deployable concept was to be applied to the spars of a telescopic wing, with two spars per wing and ribs at the end of each telescopic section. Then a covering material would join every spar and would give the wing its shape. The deployment would be achieved by compressed air contained in a high pressure canister.

The telescopic wing concept was abandoned because of the complexity of the design which included a large number of moving parts. Many of these parts could interfere and jam during deployment. It would also have been very difficult to keep the covering material taut to ensure a smooth wing surface.

3.2.2 Inflatable Wings

This wing deployment concept originated from an inflatable airplane built in 1959 by Goodyear, the model 466 / 468 "Inflatoplane" [1]. The fabric used for the wings of this aircraft is called "Airmat" which is a thick rubber constituting both the wing intrados and extrados, held together with rubber filaments to give the appropriate airfoil shape to the wing.

A Navy rapid-response surveillance projectile, similar in mission to the Wide Area Surveillance Projectile, was planning to use inflatable wings. This wing subsystem design has been contracted to the Primex Aerospace company, with which the WASP team had made contacts and had been given a rough quotation on the budget necessary for Primex to develop an inflatable wing system.

The inflatable wing concept was abandoned because of the large budget involved for contracting the wing design. In fact, it would have constituted the major part of the total project budget, and would most probably be too much. Alternatively, developing an in-house inflatable wing was not seen as the best strategy since Primex already had expertise in the field.

Appendix B contains information about the inflatable wings. Figure B1 shows the document received from the Primex company concerning the feasibility of an inflatable wing concept and Figure B2 shows an inflatable wing design.

3.2.3 Folding Wings

This wing deployment concept appeared when more doubts surfaced concerning the feasibility of the telescoping wings and the inflatable wings. The concept originated from an AIAA document [2] which described a drop test involving a glider having a 3-segment folded wing (a fixed central wing section and one folded wing tip section hinged at both ends of the central section). The deployment was initiated by gravity and by the lift generated by the sections and results show successful deployment.

Professor Mark Drela suggested that the folding wing concept should be adopted. His idea went beyond the 3-segment deployable wing glider (AIAA document described above). He suggested that the wing be a multi-section deployable wing that would, in its folded configuration, enclose the tip wing sections in between the root wing sections. The wing sections were suggested to be made of composite material with built-in metallic hinges.

This folding wing concept appeared to be a feasible and reasonably simple concept to be implemented on the flyer.

Chapter 4 Wings/Flyer Aerodynamic Development

4.1 Flyer Performance

The main flyer mission requirement was to transmit images to the ground station, for as long as possible. A derived requirement would be for the flyer to achieve steady level flight. Then some basic aircraft performance relations came into play. These were the following:

$$D = \frac{1}{2}\rho C_D V^2 A$$

$$L = \frac{1}{2}\rho C_L V^2 A$$

$$T = \frac{P}{V} \times e_p$$

For steady level flight, the following is true:

$$T = D$$

$$L = W, \text{ with } W = mg$$

Then

$$W = \frac{1}{2}\rho C_L V^2 A$$

$$\frac{P}{V} \times e_p = \frac{1}{2}\rho C_D V^2 A$$

All of the above quantities are known or can be at least bounded. However two unknowns still remain, V and A. Factoring V out of the first equation and substituting it back into the second equation and solving for A gives:

$$A = \frac{2}{\rho}\left(\frac{1}{Pe_p}\right)^2 W^3 \left(\frac{C_D^2}{C_L^3}\right)$$

The equation for A will give the wing surface area required for steady level flight. The quantities on the right hand side of the equation were uncertain and kept changing over time, which is a direct and normal consequence of the design process. For example the mass was initially set as 10 kilograms which was known to be overestimated but kept as is until enough elements had their configuration frozen. Another quantity was not exactly known for some time, that is the power of the engine. In fact the development of the propulsion system had to go through numerous analyses to find the suitable engine. A last quantity that was uncertain for some time was C_DA, for which wind tunnel testing appeared to be necessary. The other quantities were more easily estimated and closely bounded. These quantities are the air density, the propeller efficiency and the lift coefficient. Density varies little for the flyer mission altitude. The propeller efficiency could be bounded between approximately 85 and 90 percent. The lift coefficient was obtained by using the software XFOIL, and, for the selected airfoil, it can be reasonably set as 1.5 (see section 4.2 Airfoil Characteristics).

The equation for "A" was a good tool to monitor the wing surface area required to achieve steady level flight as the design parameters (weight, engine power...) were evolving through the design process. It is important to note that a wing with more surface than given by the equation would be better in that it would allow a lower flight speed which translates into a lower fuel consumption and thus more loiter time. It would also permit climbing, and thus be more flexible in terms of flight capabilities. However a larger wing area compromises the stability of the flyer because it reduces the tail volume quantity and is harder to stow.

4.2 Airfoil Characteristics

4.2.1 Wing Airfoil

The mission requirements suggested that the flyer have optimal loiter performance at one speed in the low subsonic regime. Therefore this dictates a highly cambered airfoil, from reference [3], a cambered airfoil will have a higher maximum lift coefficient and a higher lift to drag

ratio. On the downside, the ratio of maximum to minimum C_L will decrease. In this case, this is not an important concern, since the flyer will perform its mission at almost constant conditions.

The airfoil also had to be cambered and thin, for volume reasons. In fact, the stacking of the wing sections in their folded configuration dictates the choice of a thin airfoil. Section 5.1.3 discusses the wing section stacking.

The airfoil is a modified version of the T16 airfoil, which is a typical airfoil used on endurance-type model aircraft. Appendix D provides the airfoil coordinates.

The T16 airfoil was originally selected, but structural tests showed buckling of the trailing edge (see section 5.3). Therefore some modification to the airfoil was necessary: its trailing edge was thickened. Even with this modification, the airfoil shows reasonable performance, illustrated on Figure 9. This Figure shows the pressure distributions on the modified T16 airfoil for different angles-of-attack, in the flight regime that will occur during the mission. Figures 10 and 11 compare the pressure distributions on the T16 and the modified T16 airfoils at one of the most likely flight C_L values. The Reynolds number used was 158,000. This was obtained using the mean wing average chord of 0.0647 m (see section 5.4), a cruise flight velocity of 38.6 m/s (see section 4.5) and a kinematic viscosity value for a 1000-m altitude which was estimated as a reasonable mission cruise altitude.

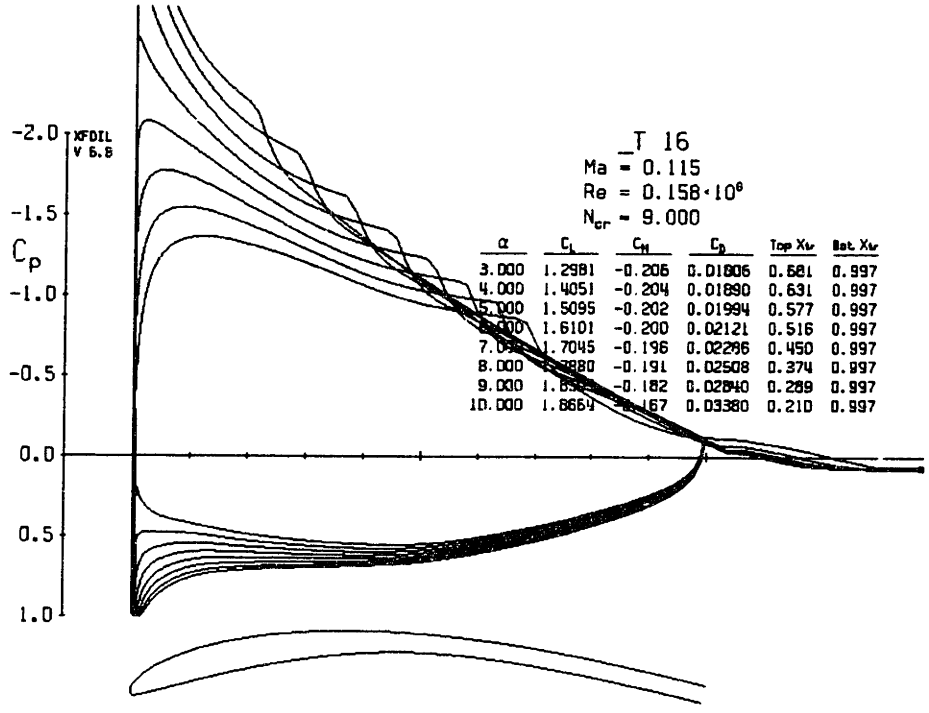

FIGURE 9: MODIFIED T16 AIRFOIL PRESSURE DISTRIBUTIONS

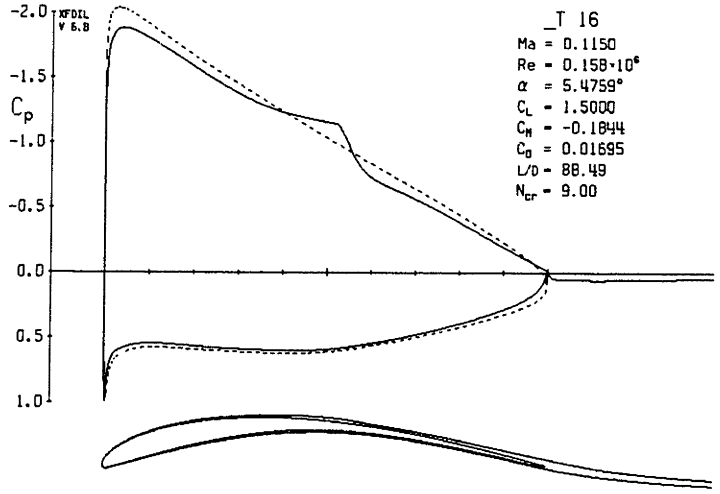

FIGURE 10: ORIGINAL T16 AIRFOIL CHARACTERISTICS

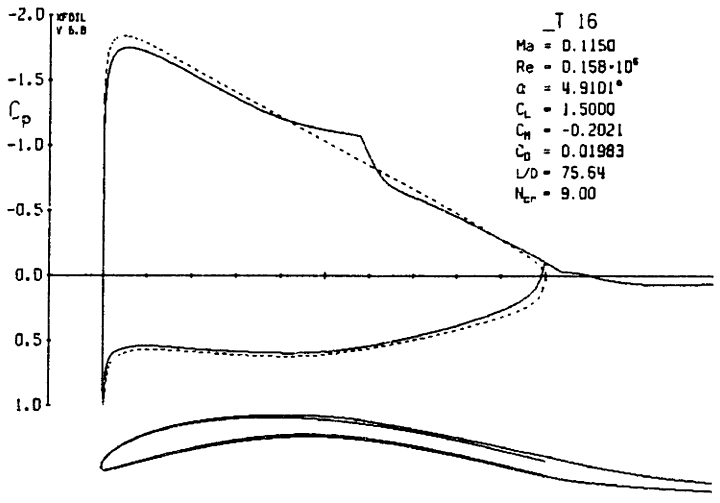

FIGURE 11: MODIFIED T16 AIRFOIL CHARACTERISTICS

4.2.2 Tail Airfoil

The tail airfoil section was selected according to two main criteria: the trim tail angle should be approximately midway between the positive stall and the negative stall, and the deflection away from the trim position should be reasonably large before stall occurs. Design iterations using the AVL and XFoil software (see section 4.3) were necessary for these respective criteria. A number of airfoil sections were analyzed, namely the NACA family 0009, 0010, 0011, and the NACA family 2411, 2413, and 2415. The best airfoil appeared to be the NACA 2413. This airfoil would be positioned up-side-down on the fuselage because the tail is down-loaded (see section 4.3.2 and Fig. 15). The trim angle was obtained as 2.2° negative deflection (upward deflection). Figures 12 and 13 show the pressure distribution on the airfoil and make it possible to identify the stall angles-of-attack. The Reynolds number used was 107500. It was obtained from the tail chord of 0.044 m [5], and the same other values as for the wing Reynolds number. Appendix D shows the airfoil coordinates. The pressure distribution results show a negative deflection stall of approximately 13.5° and a positive deflection stall of approximately 10.5°. With the trim angle predicted

to be 2.2 degrees of negative tail deflection, there would be 11.3° tail deflection from trim to negative stall and 12.7° tail deflection from trim to positive stall.

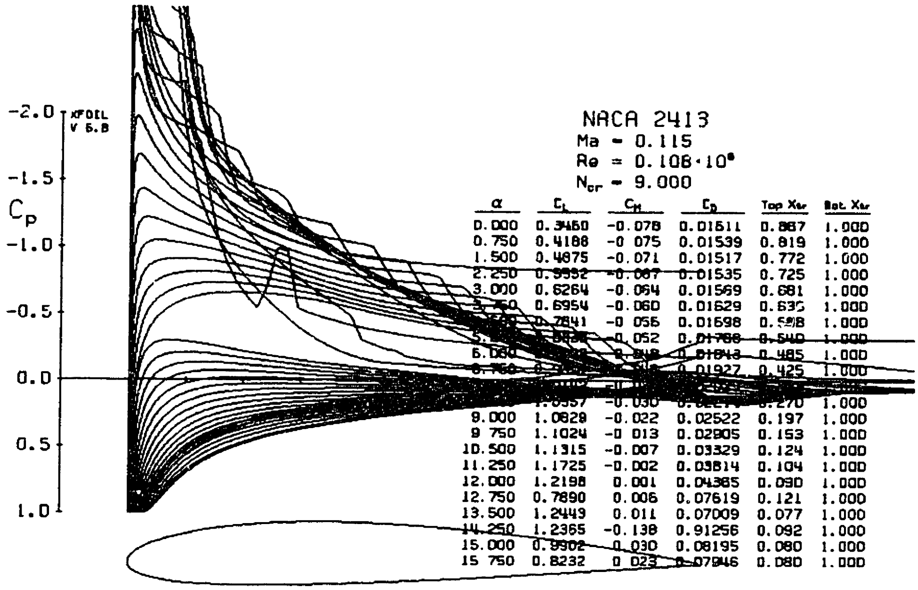

FIGURE 12: PRESSURE DISTRIBUTION ON TAIL AIRFOIL FOR NEGATIVE TAIL DEFLECTION

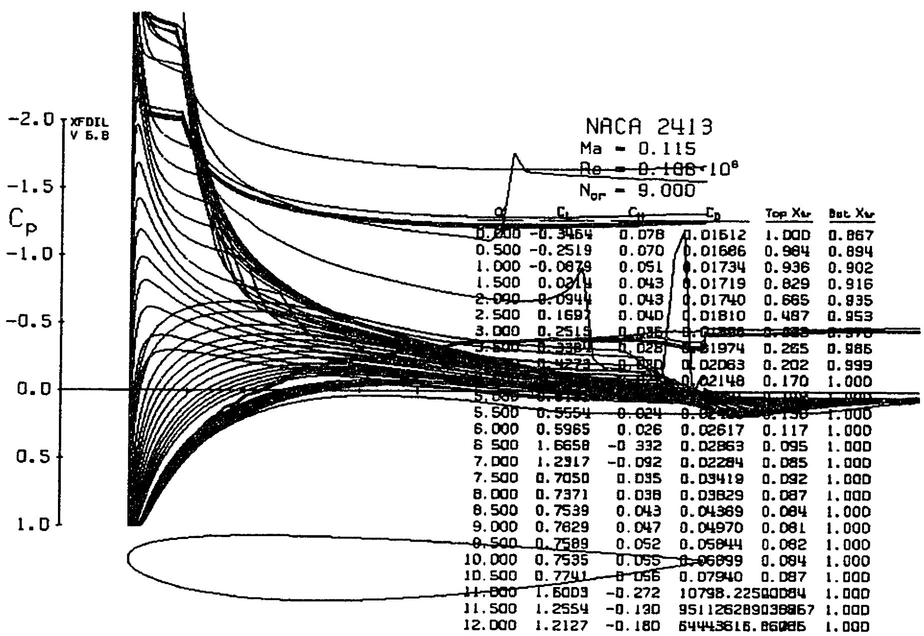

FIGURE 13: PRESSURE DISTRIBUTION ON TAIL AIRFOIL FOR POSITIVE TAIL DEFLECTION

4.3 Flyer Stability

4.3.1 Modeling

In order to determine the lift and stability characteristics of the vehicle, modeling was done using the software program AVL. This program is an application of the Vortex Lattice Method, which models the characteristics of the vehicle by distributing "horse-shoe" vortex filaments across the lifting surfaces.

The flyer modeling was modified from the file [4] created by Iranzo-Greus and Gavrilets, 1997. Appendix D provides the AVL input code.

Many design iterations were performed using the model during the length of the flyer development. The geometry of the flyer needed frequent updates especially in the early design phases before the illuminating round-internal flyer concept was chosen. The model made it possible to study and to establish stable configurations while the aerodynamic surfaces where changing in geometry throughout the design phases. Figures 14(A) and 14(B) show typical AVL configuration views.

4.3.2 Stability derivatives

The dynamic stability characteristics of an aircraft can be described in terms of stability derivatives. These are derivatives of forces and moments acting on an aircraft with respect to angles and rotation rates. Although there are 36 derivatives, only 13 of them are meaningful once longitudinal and lateral-directional dynamics have been decoupled.

AVL was used to obtain the stability derivatives. These derivatives are expressed in NASA standard axes with X forward and Z down. Table 1 summarizes the results for the final flyer configuration shown by Figures 14(A) and 14(B).

TABLE 1: FLYER STABILITY DERIVATIVES

alpha (rad)	beta (rad)	roll rate p	pitch rate q	yaw rate r
CLα = 6.84444	CYβ = -1.08684	CYp = -0.02133	CLq = 9.63739	CYr = 0.05912
Cmα = -0.72045	Clβ = -0.01114	Clp = -0.00768	Cmq = -12.3658	Clr = 0.00433
-	Cnβ = 0.00117	Cnp = -0.00158	-	Cnr = -0.00103

From the table, it can be seen that the aircraft is longitudinally stable. This is shown by the negative static margin (Cma divided by CLa). A reasonable value of 10% is also reached. However this value is attained when the fuel tank if full. The fuel tank being ahead of the center-of-gravity (CG), this static margin value drops from 10% to approximately 6%, when the fuel tank is empty. The signs of the other derivatives show stable behavior.

The final CG position is set at 0.208 m from the base of the flyer.

Before arriving at this final configuration, a number of design decisions were made. The most important and perhaps the most interesting of these are the following.

The wings were originally set almost two inches forward along the fuselage longitudinal axis compared to their final location. This wing position needed a CG approximately two inches further to the front of its actual position to create a stable flyer configuration. This forward wing position was not compatible with the natural structural weight distribution of the flyer, which implied adding a substantial amount of ballast in the nose of the flyer. This mass amounted to approximately three pounds. The decision was then taken to bring the wings further back along the fuselage. However the limiting factor was the tail volume quantity, and the need for enough longitudinal stability. The wings were brought back, where the stable CG position corresponded to the natural structural CG position, and this resulted in a tail volume of 0.53. This last value seemed somewhat small, but the dynamic longitudinal response was found to be reasonable [6]. The two flyer downward pointing control surfaces had their area and pointing angles set by the internal geometry constraints of the tail module. One stability derivative was still unstable, that is

the Cnb yaw derivative (negative value). The problem was solved by adding two vertical fins (see Figures 14(A) and 14(B)) that were able to give a positive value to the Cnβ derivative. Space was found at the back of the tail module to incorporate these two fins as well as their deployment mechanism.

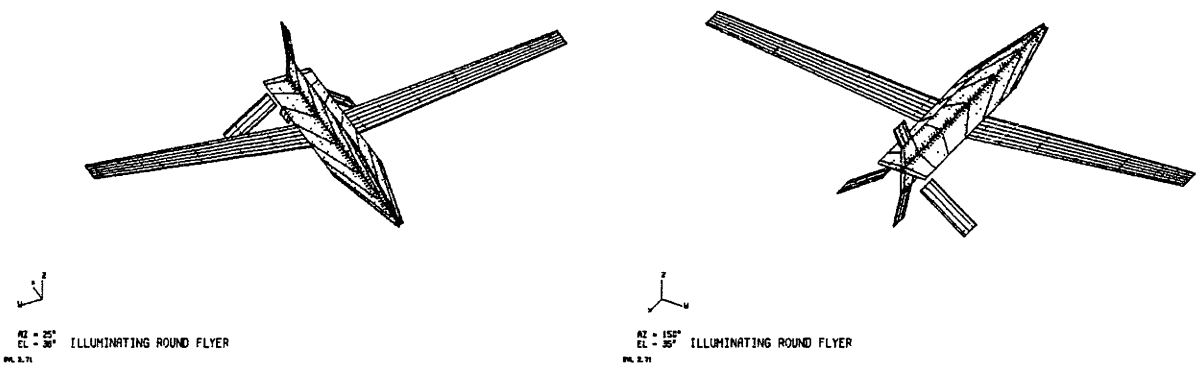

FIGURES 14(A) AND 14(B): VIEWS OF THE FINAL AVL CONFIGURATION MODEL

Figure 15 shows the Trefftz Plane Loading where the local section aerodynamic loading can be seen. This Figure shows the quasi-zero angle-of-attack of the fuselage during cruise conditions (α on the Figure). It also shows the downward load on the tail. The conditions are trimmed conditions (CM = 0).

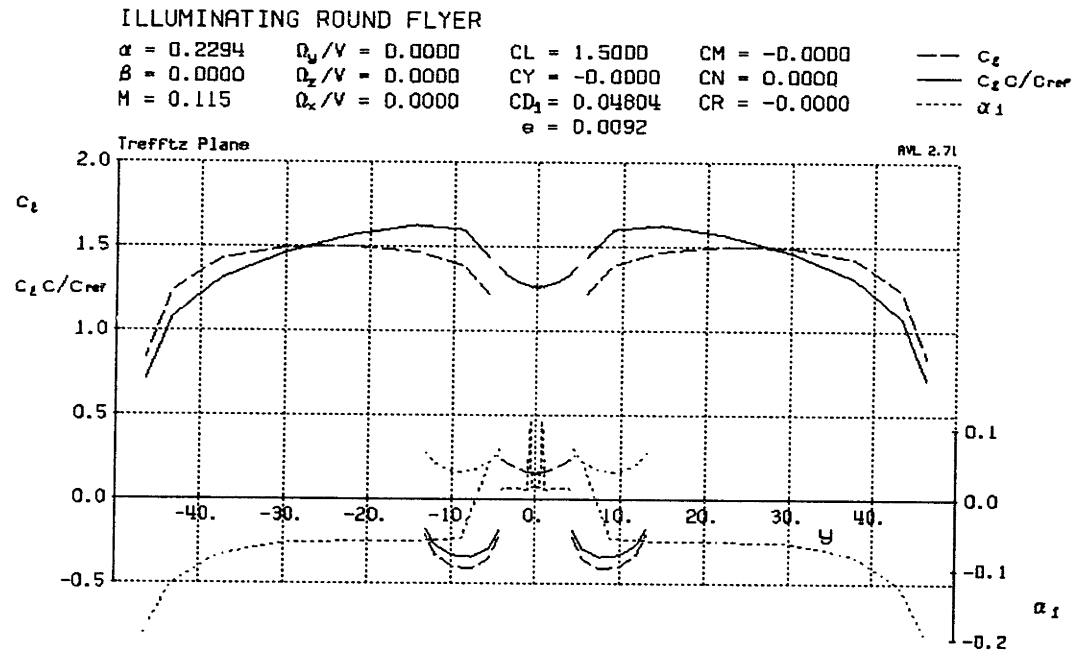

FIGURE 15: TREFFTZ PLANE LOADING

The characteristics of the final configuration are the following:

- Wing:
  - Area (excluding fuselage): 0.0553 m^2
  - Total span (including fuselage): 0.923 m
  - Sweep angle: 0^o
  - Incidence: 7^o
  - Design lift coefficient: 1.5
  - Dihedral angle: $4\text{-}6^o$
- Tail:
  - Dihedral angle: -35^o
  - Incidence for trim: 2.2^o
- Length of flyer: 0.52 m
- Tail volume: 0.53
- Static Margin: 5% - 10% stable

4.4 Wind Tunnel Testing

Wind tunnel tests were conducted to get accurate drag data for the body. In fact, the latter incorporates cavities where the wings are stowed for the ballistic portion of the mission. When the wings deploy, there is a void in the body in front of the wings. This complicates its geometry and analysis so wind tunnel testing was found appropriate for drag analysis. The drag results are useful to determine the engine power requirements and to characterize the flyer performance.

The measurements were conducted in the 5' X 7' MIT Aeronautics and Astronautics wind tunnel. This wind tunnel has an open section of the above dimensions and has a wire balance measurement system. Three wires were used for the experiment: one drag wire in the front, one lift wire, and one moment wire at the rear. The angle-of-attack was easily set at a desired value by raising or lowering the moment wire.

The setup used is sketched on Figure 16. Figure 17 shows a picture of the test model.

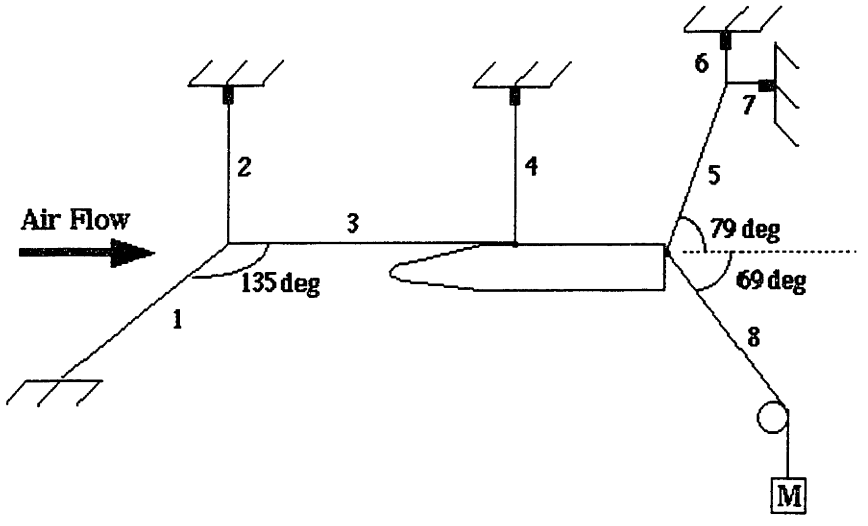

	Length (cm)
1	107
2	81
3	79
4	81
5	109
6	10
7	8
8	80

FIGURE 16: WIND TUNNEL MODEL SETUP

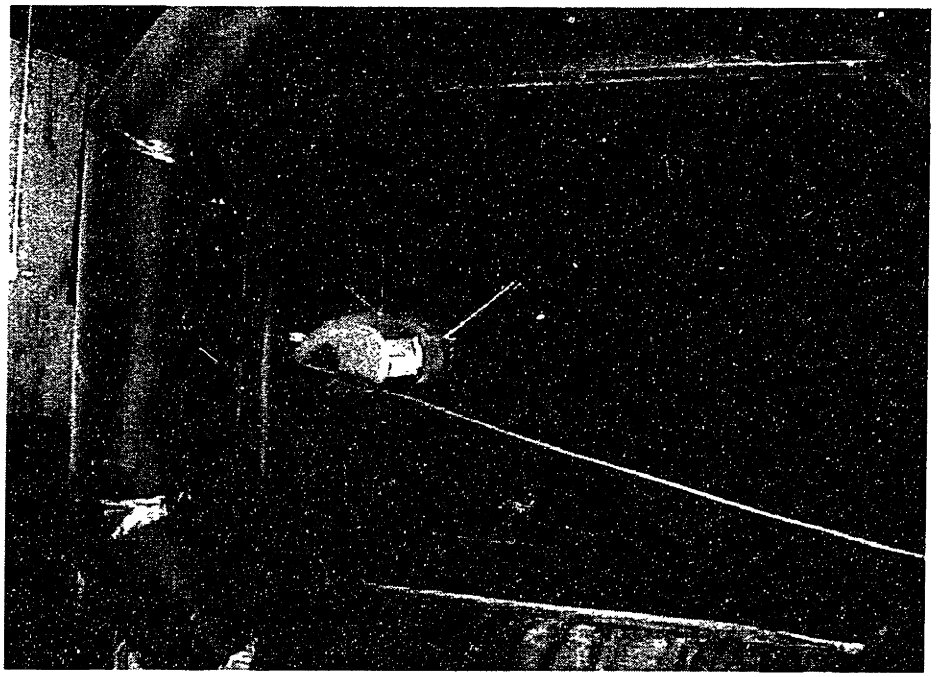

FIGURE 17: WIND TUNNEL TEST MODEL

The model to be tested in the wind tunnel did not have a pair of wings ready for the experiment. It was thus tested with only the body and the tails. Drag contribution for the wings was obtained analytically and added to the experimental body and tail drag data. To obtain accurate experimental data, the drag of the wires had to be subtracted from the measurements taken with the model in place in the tunnel. The setup for measuring the wire drag data was obtained by removing the model and placing a thin rod in lieu of the latter.

Results are presented in terms of

$$C_D A = \frac{2D}{\rho V^2}$$

Where D is the drag force directly obtained from the load cell at the top of wire # 2 and V is the tunnel air speed. Therefore, the quantity on the right hand side is directly measurable in the wind tunnel. The left hand side shows the results in terms of $C_D A$, which has more value than just a drag coefficient, because $C_D A$ is not yet referenced to an area.

Since the wind tunnel maximum velocity was below the predicted flyer velocity, some trend in the results was necessary to predict drag characteristics at higher velocities. C_DA was thus presented versus velocity (see Figure 18). The body was set with zero angle-of-attack with respect to the flow and the tails are set with a four degree negative angle of incidence. These angle settings represented the predicted trimmed flight conditions at the time of the test, which is close to the final approximated trim angle value (2.2^o).

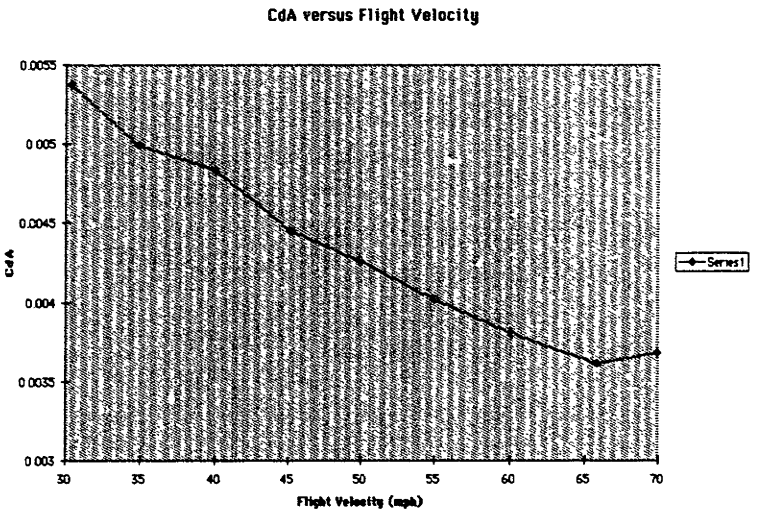

FIGURE 18: C_DA VERSUS FLIGHT VELOCITY FOR BODY AND TAILS

Knowing the final wing area, it was interesting to have an idea about the value of the drag coefficient. Figure 19 presents the drag coefficient referenced to the wing area. Here again these numbers refer to an experiment performed with only the body and the tails. The body is also set at zero degree angle-of-attack in this test and the tails at a negative four degrees angle.

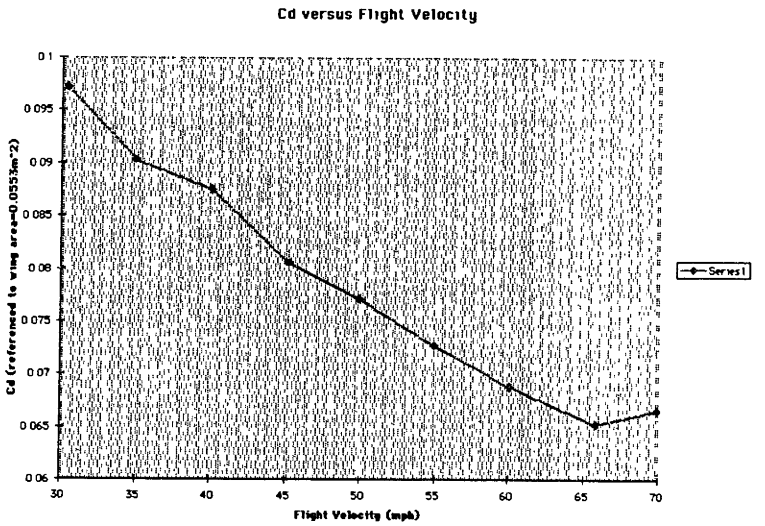

FIGURE 19: C_D VERSUS FLIGHT VELOCITY FOR BODY AND TAILS (BASED ON WING AREA)

Experiments were also performed with the body alone and drag coefficient data was reduced with reference to the body cross-sectional area which can be of interest. The results are presented on Figure 20.

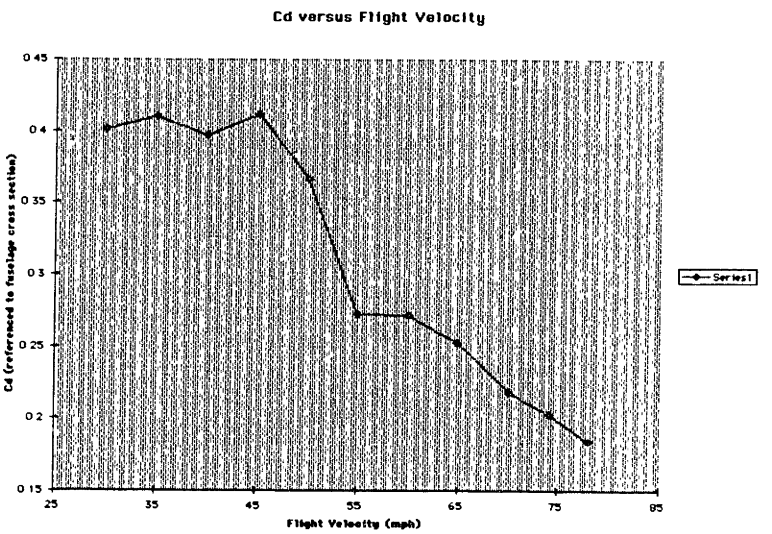

FIGURE 20: C_D VERSUS FLIGHT VELOCITY FOR BODY ALONE (BASED ON BODY CROSS-SECTIONAL AREA)

4.5 Some flyer Aerodynamic characteristics

Here, an attempt is made to calculate the flyer Lift over Drag (L/D).

Wing area was set at some point in the structural wing design when the latter had to be frozen in order to carry on development. The design was frozen while some flyer parameters were still not determined precisely, such as the total weight, the fuselage drag, and the engine power. Both wings then totaled a surface area of 0.0553 m^2. The final flyer weight was then established to plus or minus five percent as seven kilograms. Thus with these values in hand it was possible to calculate the flight velocity using the relations presented in section 4.1. Using the previous values and values for the air density of 1.1121 (at 1000 meters altitude, a reasonable mission altitude), C_L of 1.5 for the wings, a flight velocity of 38.6 m/s was obtained.

To get a good estimate for the drag, wind tunnel data had to be extrapolated since the C_DA values were obtained for velocities of only 70 miles per hour which corresponds to 31.3 m/s, whereas 38.6 m/s (the flight velocity) corresponds to 86.3 m.p.h. Using Figure 18, and extrapolating, for a flight velocity of approximately 86 m.p.h., a C_DA value of approximately 0.0035 could be estimated. This C_DA value corresponds to the body with the two tails only. Since the wings were not tested in the wind tunnel, it was necessary to rely on analytical data to obtain their C_DA contribution. This contribution is divided in two parts: the induced drag contribution ($C_L^2/\pi Ae$) and the profile drag contribution (obtained from the XFoil program. Induced drag contribution was $C_L^2A/\pi ARe = 0.0032$, where AR is the aspect ratio, (AR = 12.95), and e is the Oswald efficiency factor, (e = 0.95). the profile drag contribution was obtained from Figure 9, where C_D = 0.02. Multiplying by A gives 0.0011. The total wings C_DA contribution was thus 0.0043 m^2. For the total flyer, the C_DA could then be obtained and totaled 0.0078 m^2. Finally the drag was obtained as 6.46 Newtons. This resulted in a L/D of 10.63.

The thrust value could then be compared to the drag value. $T = 745Pe_p/38.6 = 7.05$, with 745 being the conversion from horsepower to watts, P being the maximum engine power of 0.42

hp (see section 7.1), e_p (propeller efficiency) taken as 0.87, and 38.6 being the cruise flight velocity.

From the last calculation, it appears that the thrust is slightly higher than the drag, for the engine at peak power. This implies that the flyer could actually climb during its mission, or achieve steady leveled flight with an engine power setting less than the maximum setting.

In performing these calculations, a number of assumptions and limitations are worthwhile mentioning:

- The additional drag due to the hinges and the springs under the wings (see chapter 5) was not taken into account (Approximated to be equal to 0.271 Newton at cruise velocity)
- The two small vertical fins at the back of the flyer were not modeled (Approximated to be equal to 0.00497 Newton at cruise velocity)
- Interference drag between the wings and the body was not taken into account

Chapter 5 Foldable Wings: Structural / Geometric Development

5.1 Mechanisms Design

5.1.1 Available Wing Packaging Volume

The two wings have a central location on the flyer. They occupy the largest volume of the wing module. The volume and dimensions available to store the wings are:

- Volume: 7.22 x 10^{-4} m^3 (44.08 in^3)
- Length: 0.13 m (5.118 in)
- Height: 0.06 m (2.362 in)
- Radius: 4.95 x 10^{-2} m (1.95 in)

Figure 21 shows the cavity representing the space available for packaging the wings (the wing cavity). Both wings, including every deployment mechanism must occupy no more than this cavity volume.

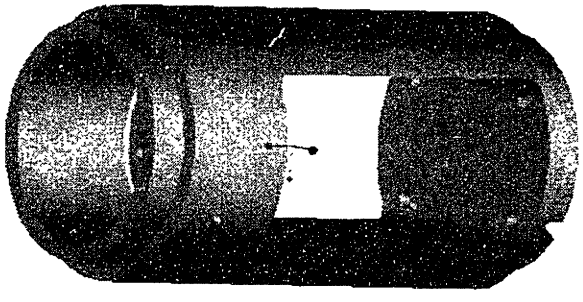

FIGURE 21: SPACE AVAILABLE IN WING MODULE FOR WING PACKAGING

5.1.2 Pivot Design

In order to free the wings from the wing module cavity during deployment, the wings execute a 90° rotation about a pivot point. Figure 22 represents a top view of the wings deploying out of the wing module cavity by pivoting around a pivot point. After the 90° pivot motion, the leading edge of the wing faces the flow.

The concept of the pivot came from the observation that the wings would have more chances to survive the high-g environment if the spanwise direction of the wing was aligned with the fuselage longitudinal axis. Then the structural problem would be one of curved shell buckling. Since the airfoil section to be used has a relatively short radius of curvature, the buckling characteristics were expected to be good, with the acceleration loads applied through the airfoil shape cross-sectional area. The buckling characteristics of a wing stowed with the leading edge facing the front of the flyer would be much worse. In fact, the acceleration loads would be transmitted through this wing configuration as a plate/column with an initial imperfection. Moreover, with the wing stowed in this configuration, the loads being applied through the thin trailing edge will create high local stresses.

The pivot concept has a storage space efficiency drawback. Looking at Figure 22, it can be seen that the tip of the wing has to clear the edge of the wing box when pivoting out. This limits the wing geometry such that in its stowed position the corner of the wing must remain within a limit shown by a dotted arc on the sketch. Increasing the wing chord would reduce its span and vice-versa.

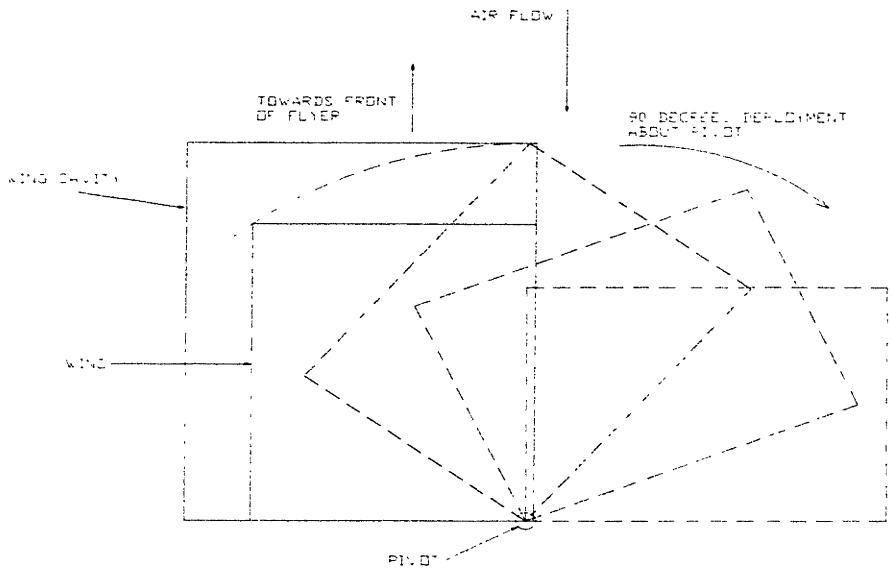

FIGURE 22: PIVOT DEPLOYMENT CONCEPT

To allow the wing to pivot 90° out of the wing cavity, the concept of a "wing arm" was introduced. This arm is the junction between the pivot shaft and the wing. A "back wing support" plate holds the pivot shaft and is fastened at the rear end of the wing box to the flyer. The acceleration (g) loads are transmitted from the wing through the wing arm through the back wing support to the flyer. The rotation around the pivot shaft is insured by the use of a torsion spring located at the center of the shaft and around it. This spring is held by both the back wing support and the wing arm.

Figures 23(A) and 23(B) show views of the pivot mechanism, the back wing support, the wing arm and a portion of the wing (the right wing in this case).

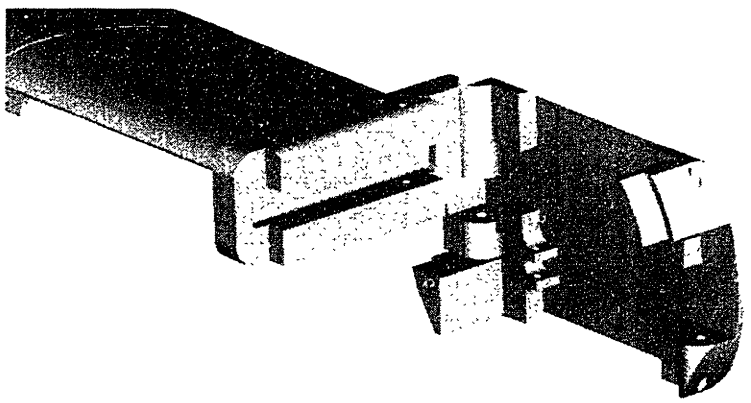

FIGURE 23(A): VIEW OF PIVOT MECHANISM (FROM INSIDE OF WING CAVITY)

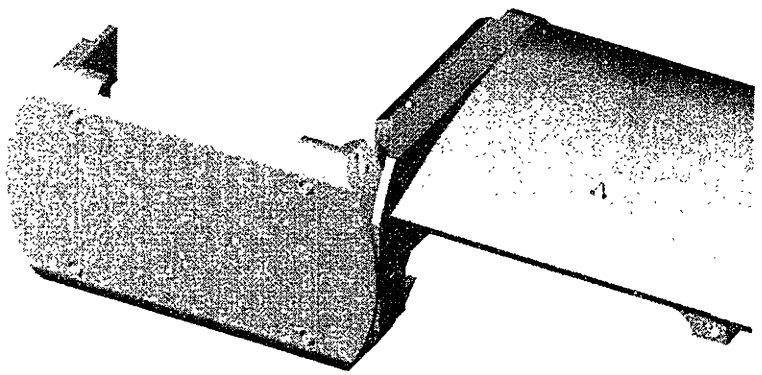

FIGURE 23(B): VIEW OF PIVOT MECHANISM (FROM OUTSIDE OF WING CAVITY)

5.1.3 Wing Sections Stacking

In order to determine the number of wing sections (or segments) and their different chord lengths that can be stacked in a given set of dimensions, the software Airset [7] was used. Airset proved to be an efficient geometry tool and permitted accurate evaluation of the wing section stacking. Figure 24 shows an example use of Airset. From the wing cavity available volume, six segments per wing was found to be a feasible and reasonable number. With six segments the wing area requirements for steady level flight were also met. Section 6.4.1 and Table 6 present the dimensions of each segments.

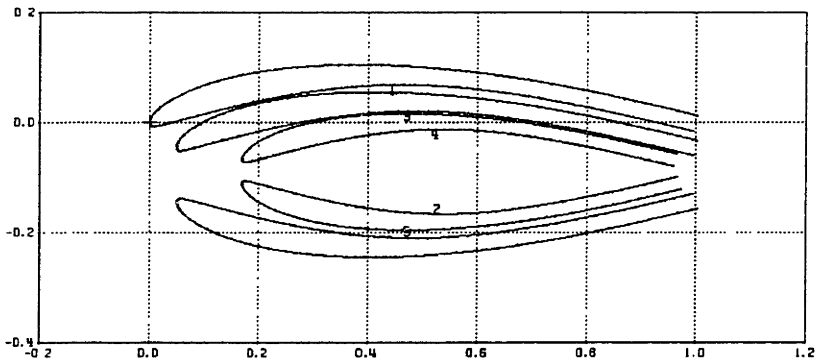

FIGURE 24: WING SECTIONS STACKING

5.1.4 Hinge Design

Once a stacking configuration was established with Airset, the link between the wing sections was insured through the use of hinges. A number of requirements were to be applied to their design, and are discussed in the following. The hinge had to be designed so as to enable a 180° rotation of a wing section relative to the one connected to it. It also had to provide an aerodynamically clean top wing surface for aerodynamic efficiency, imposing the hinges to be located under the wing sections. Also, when the wing deploys, the top surfaces of each section must be continuous, thus imposing the hinge line to be midway between two adjacent wing sections (in cross-section view). Furthermore, the hinges must prevent two adjacent wing sections from translating longitudinally. Finally the hinges must provide space for a torsion spring, that would contribute to the deployment of the wing. Figure 25 shows a hinge between two wing sections, with the leading edge appearing at the bottom right. A space is intentionally left at the center of the hinge to insert a torsion spring mounted around the hinge shaft. The front end of the hinge is streamlined to help reduce drag. The interface between the hinge and the wing sections is made through a generous round to help reduce stress concentrations.

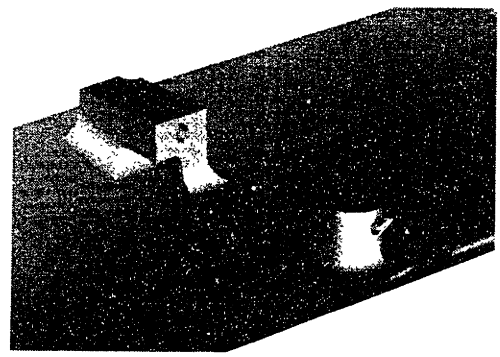

FIGURE 25: HINGE BETWEEN TWO WING SECTIONS

5.1.5 Spring Characteristics

Torsion springs were found to be a good candidate to deploy the six wing sections of each wing. Although the aerodynamic pressure on the wing could help deploy the wing, the torsion springs were required to ensure a proper and reliable wing deployment. As a requirement for the springs, it would be necessary for the wings to deploy and to stay deployed (statically), thus supporting at least their own weight.

The development of the springs was done concurrently with the hinge geometry layout. The diameter of the springs determined the width of the hinges, as the sides of the hinges were required to be aligned with the outer diameter of the springs to help streamline the hinge-spring setup, and thus to help reduce drag.

The springs were mounted around the hinge shafts in the center of the hinges. Such a central position increased the volume available to fit the spring due to the high camber of the wing.

Five springs were required to support one wing with reducing torque requirements from wing root to wing tip. The torque requirements were obtained from the lengths of the wing sections, together with their weights. Since the wing, in its deployed configuration, would have to support its weight, the springs would need to be in tension and would need to allow an added 180^{o} rotation without yielding, to bring the wing in its stowed configuration. The springs would then

need to rotate more than 180° without yielding, to provide enough torque when unwound 180° (deployed wing) from its maximum wound state (stowed wing). They would also need to satisfy maximum length and outer diameter given by the hinge geometry and to have a small outer diameter for a small frontal area for drag considerations. A MATLAB program was created to find the wire diameter that would satisfy all of the above constraints (see Appendix D). This program made use of torsion spring design relations found in [7]. An output example of the program is shown on Figure 26, where the top of the curve gives the optimum wire diameter. The spring would then be completely defined, with the wire diameter, the number of turns, the outer diameter, and the angle to wind it when putting it in place under the wing. Table 2 summarizes the spring characteristics. The spring numbering is from wing root to wing tip, thus spring 1 is intended for the hinge between wing section 1 and wing section 2, spring 2 between wing section 2 and wing section 3, and so on. These characteristics are intended for springs with more torque than required by approximately 20-40%. The springs were manufactured and proved efficient. A picture of the springs mounted under the wing is shown on Figure 37.

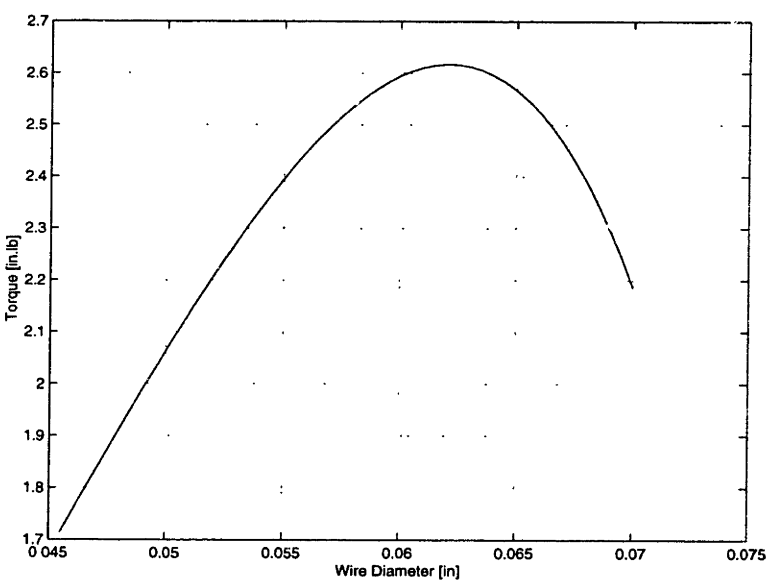

FIGURE 26: SPRING PROGRAM OUTPUT EXAMPLE

TABLE 2: SPRINGS CHARACTERISTICS

Spring #	Deflection Angle (deg.)	Coil O.D. (in.)	Wire dia. (in.)	Number of Coils
1	330	0.500	0.062	14.8
2	340	0.350	0.052	18.8
3	340	0.270	0.041	19.3
4	340	0.200	0.033	21.3
5	350	0.150	0.021	17.6

5.2 Structural Analysis

5.2.1 Material Selection

The original suggestion to manufacture the wings using composite materials with metallic hinges was abandoned. This decision was based on problems associated with binding composites and metal. Moreover, the tight time frame of the project directed the wing development towards functionality rather than performance. The decision was then made to use an aerospace-grade aluminum (7075) for the entire wing manufacturing. All-aluminum wings are heavier and probably less stiff than composite-metal wings, but easier to manufacture.

5.2.2 Launch Loading Case

Since the wing stowed geometry configuration was established to offer good set back g resistance, the concern arose as to whether the wing could survive the estimated 4000 g set forward acceleration. Finite Element Modeling (FEM) of the root wing section was performed (all the Finite Element Modeling Analyses in this section were performed by engineers at the Draper Laboratory), with 4000 g's multiplying the sum of the five remaining wing section weights. Acceleration loads would be applied through the hinge of the first wing section. Figure 27 shows

the stress levels on the latter. More load was applied to the front part of the hinge, since the wing section center of gravity is towards the front on the section. Stresses obtained are the highest at the base of the hinge front part. At that point, the stress is almost twice as high as the yield stress of the 7075 aluminum selected for the wings (7075 Aluminum yields at approximately 78,000 psi).

To solve this problem, a support had to be designed so the loads could be transferred to the rest of the flyer and ease the high values of stress at the first hinge location. A block was inserted on top of the stowed wing, without preventing its deployment. Its shape was dictated from the arc describing the opening of the wing and the wing itself. The vertical edge of the block is aligned with the flyer exterior. Figure 28 describes the geometry and deployment sequence of the wing-block arrangement.

FIGURE 27: STRESS AT SET FORWARD ON ROOT WING SECTION

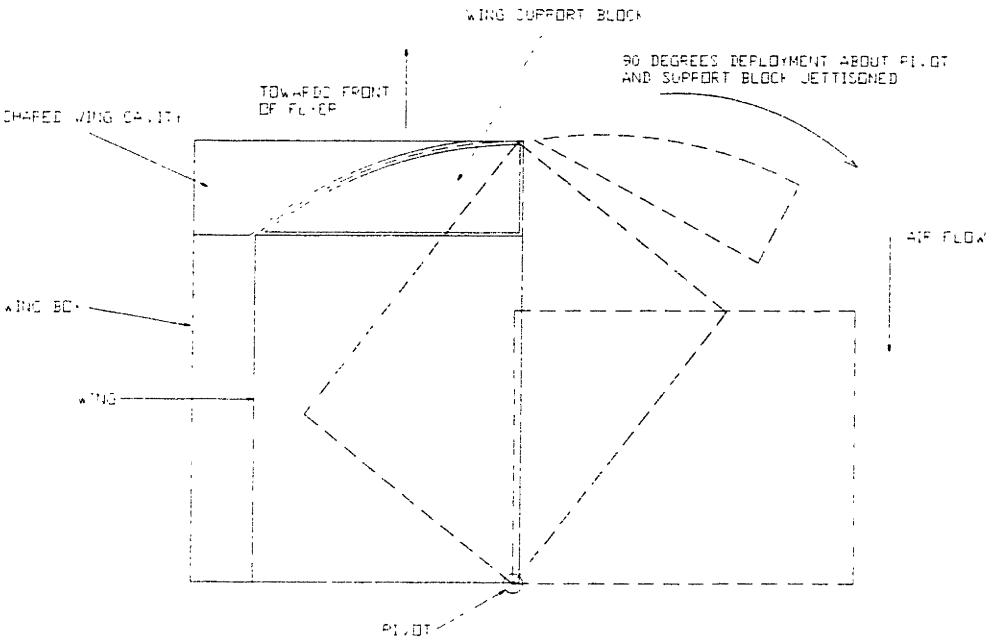

FIGURE 28: GEOMETRY OF WING SUPPORT BLOCK

5.2.3 Flight Loading Case

The final wing design was analyzed in its deployed state to establish the maximum flight velocity or the maximum maneuvering loading the wings could sustain.

Figures 29, 30 and 31 show stresses at the root of the wing and at the pivot attachment respectively, subjected to a steady level flight wing loading. A load of 34 N (one wing is loaded with half of 7kg X 9.81 N/kg =34 N) was applied at the mean average chord location along the wing (0.213 m from the wing root). The maximum stresses occurred at the wing root and at the pivot attachment. It is interesting to note that these stress values are approximately the same at the wing root and at the pivot attachment. From all three pictures, the maximum stresses were approximately 9000 psi, which is almost nine times less than the yield stress of the 7075 aluminum. This meant that a maximum of nine-g loading would be allowed on the wing, or that a maximum flight velocity of three times (loading increases with the square of the velocity) the cruise velocity would be allowed.

Figure 29 shows the highest stresses at the leading and trailing edges of the wing, and on this Figure, the wing design shows no round between the undersurface of the wing and the wing arm. Adding a round would increase the loading capabilities and this round was included on the machined metal wing. Figures 30 and 31 show unacceptable stress concentrations around the pivot structure. This structure was therefore redesigned including rounds where possible in the high stress areas, to reduce the stress values.

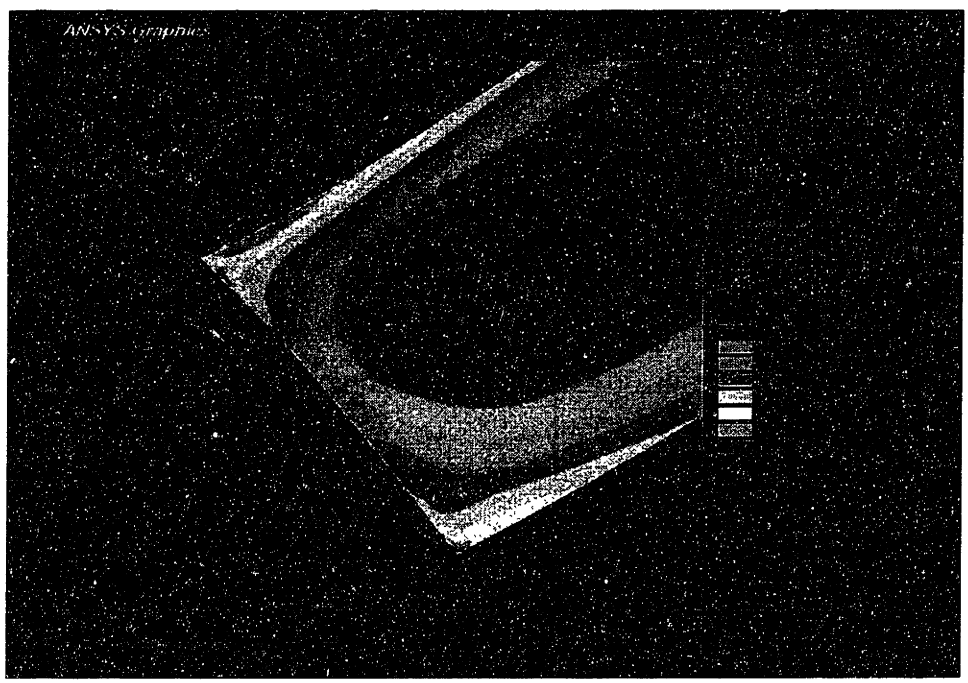

FIGURE 29: STRESSES IN FLIGHT, WING BOTTOM

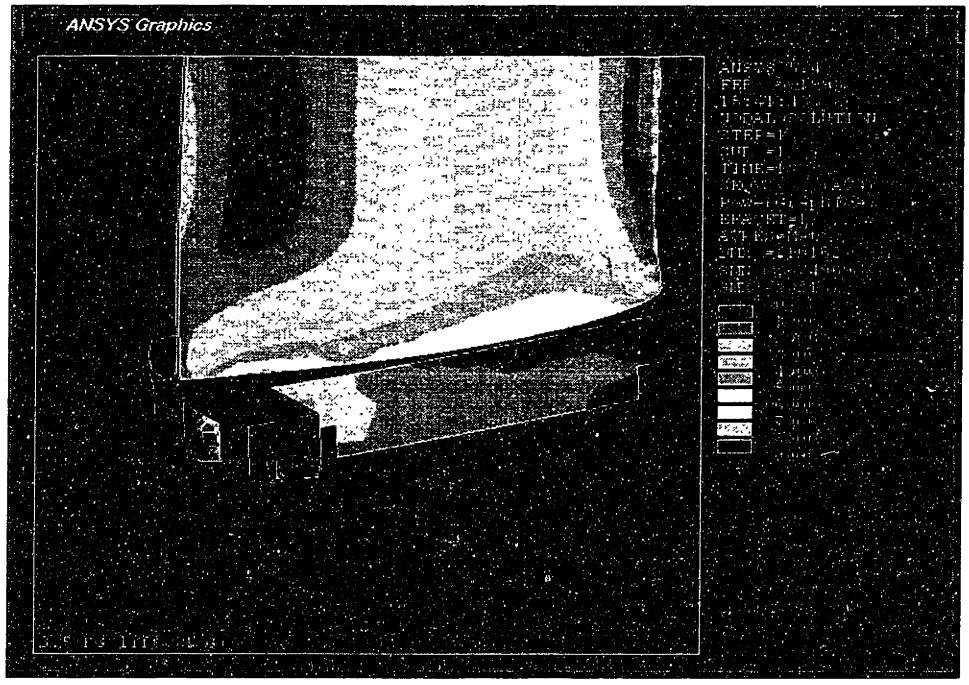

FIGURE 30: STRESSES IN FLIGHT, WING TOP

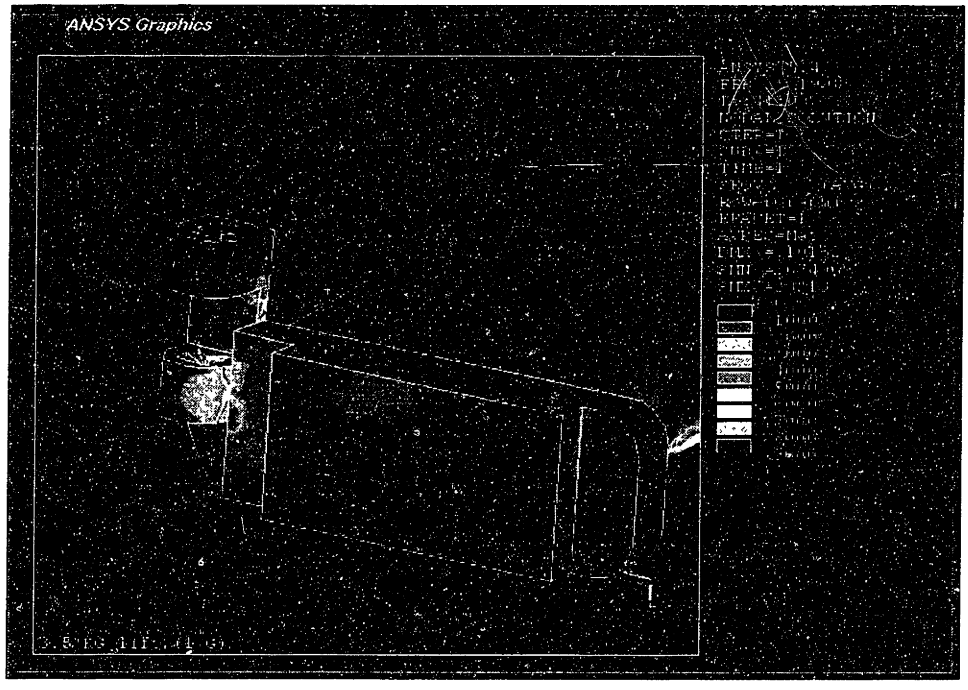

FIGURE 31: STRESSES IN FLIGHT, PIVOT

5.3 High-g Tests

High-g tests were performed to validate the wing design at the Picatinny Arsenal in New Jersey. There, a 5-inch air gun was used for canister tests. The Picatinny air gun tests were provided at no cost, and a total of 28 tests were conducted. Figure 32 shows the 5-inch air gun. This was originally a conventional gun barrel that was modified into an air gun. A long tubular extension was added to its muzzle to allow for the deceleration of the test article. A pressure of a few hundred psi was kept in this tube in order to decelerate the test item and to send it back to its starting point, where it is unloaded. This feature eased and quickened the testing operations. Many tests could be conducted in a given day.

The air gun can reach the same high-g accelerations created by a real gun launch, but the acceleration pulses are different. In fact, the air gun accelerated the test canister to 15,000 g's in approximately 1 millisecond, whereas a real gun accelerates an object to 15,000 g's in approximately 17 milliseconds. Figures C1 and C2 show the acceleration chart for the air gun and a real gun. So it is recognized that a test article surviving 15,000 g's in the air gun for one millisecond may not survive the same load spanning a longer time interval.

Figure 33 shows a typical air gun canister in which a test item is inserted. The canister is then inserted into the gun.

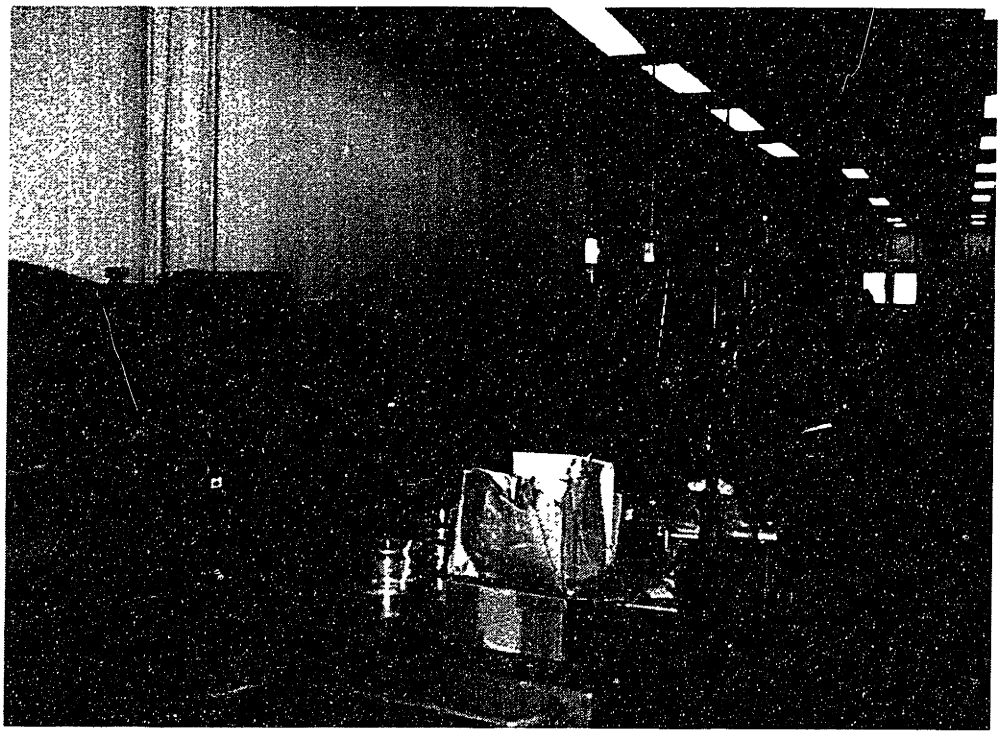

FIGURE 32: THE 5-INCH AIR GUN FACILITY AT PICATINNY ARSENAL

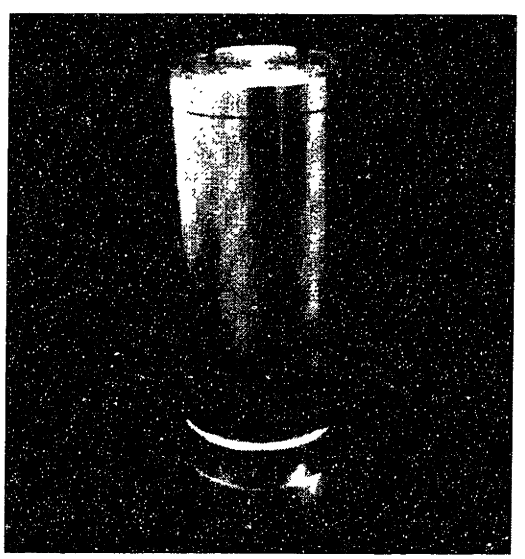

FIGURE 33: TEST CANISTER

5.3.1 Pivot Test

The first wing air gun test sequence had the goal of validating the pivot design. These tests occurred in the early wing design phases when the pivot design was already frozen and a first wing section was manufactured in one part including the wing arm and the pivot structure. A small section of the original T16 airfoil was included at the root of the wing section and a block representing the weight of the additional wing sections was added on top of this portion of wing section (see Figure 34).

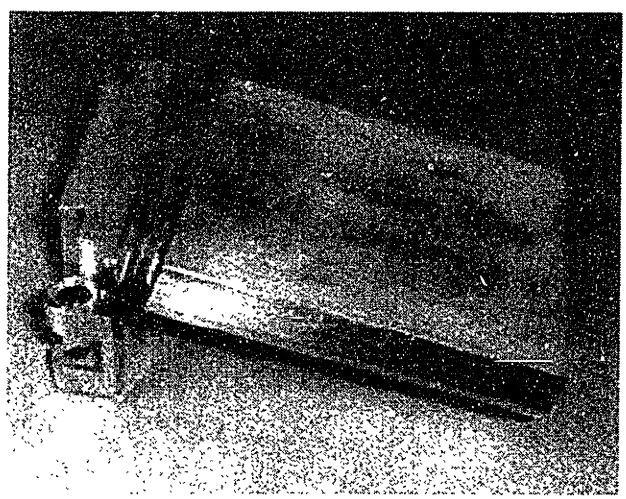

FIGURE 34: PIVOT TEST ARTICLE

Three tests were conducted, with varying g loading and visual checks were made at the end of each test. Table 3 summarizes the test results.

TABLE 3: PIVOT TEST RESULTS

Test	G Load	Results
1	1400	No pivot damage
2	4962	No pivot damage, Wing slightly bent
3	15100	No pivot damage, wing buckled

The conclusions of the *pivot* air gun tests were the following. The pivot structure showed no damage and functioned as well as before the tests. However, damages were noted on the wing section. This section buckled at the trailing edge. This section included the original T16 airfoil which had a cusp trailing edge, and did not survive the high-g environment.

An airfoil trailing edge redesign was then performed, by thickening it, starting near the leading edge, to blend the added thickness smoothly through the entire chord of the airfoil. The thickness was increased based on NASA documents on the buckling of curved shells [8] and also based on the eventuality of a deployment of the first wing section at transonic speeds, a condition which the flyer deployment sequence was predicted to start. The trailing edge thickness was then increased to 2.3 millimeters. All other sections also had their trailing edge thickened.

5.3.2 Hinge Test

The goal of the second wing air gun test was to validate the hinge design. Two parts composed the test article, one being the wing arm and a full first wing section, and the second part being a small segment of wing section with a block representing the weight of the remaining five wing sections. These two parts were linked by a hinge, with protuberances on both parts. The block on the second part was not resting on the wing arm but a shim was inserted between the block and the wing arm to ensure contact between these parts. Having contacts between every wing section and the wing arm was the design intention. This allows load transfer from the wing sections to the wing arm. As a requirement for manufacturing the shim, it was necessary to have the same contact area on the wing arm as the hinges on the tip of the second wing section. Figure 35 shows the hinge test article. In this Figure, the modified T16 airfoil section developed from the original T16 section can be seen (Figure 34).

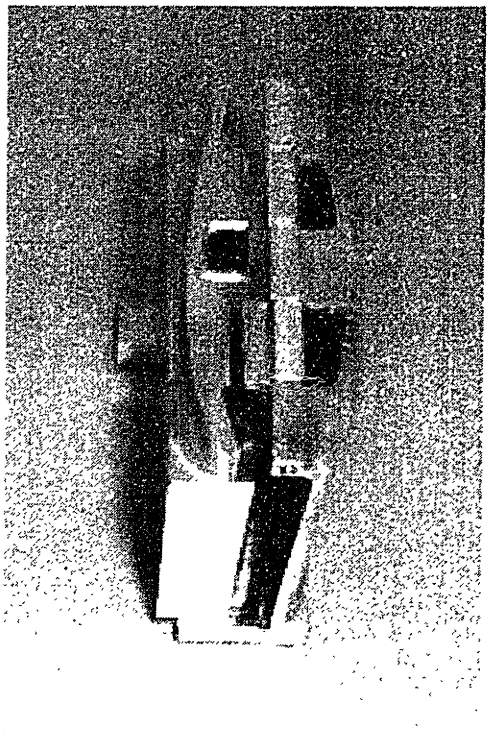

FIGURE 35: HINGE TEST ARTICLE

Four tests were conducted, with varying g loading and setups. Table 4 summarizes the test results.

TABLE 4: HINGE TEST RESULTS

Test	Support	G Load	Result
1	yes	6000	No visible damage, no hinge resistance
2	yes	12313	No visible damage, no hinge resistance
3	yes	14270	No visible damage, no hinge resistance
4	no	11302	Hinge failed

Conclusions for the *hinge* air gun tests were the following. The hinge showed no damage and no added rotation friction even at the highest g loading condition, provided the shim was in place. The contact between every wing section and between the second wing section and the wing arm is thus crucial to improve survivability at high-g loadings.

5.3.3 Integrated Wing Test

A final air gun wing test sequence was performed with a wing including the wing arm and the six wing sections connected together and springs between every section. The wing could be used as a final prototype wing, for a real flyer mission. This wing incorporated the design changes motivated by the lessons learned during the two previous air gun tests. Table 5 summarizes the test results.

TABLE 5: INTEGRATED WING TEST RESULTS

Test	Load Direction	G Load	Result
1	Set back	7536	No damage
2	Set back	14883	No damage
3	Set forward	3673	No damage

The wing survived all test configurations and conditions. The decision was then made to manufacture the second wing identical to the first one, and to integrate the wing subsystem in the flyer in preparation for the fully integrated test of the whole system using the 8-inch gun canister test system at the Navy's Dahlgren facility (see Chapter 7).

5.4 Final Integrated Wing

The final integrated wing is presented in this section, showing the layout with the six wing sections assembled and the deployment scheme.

5.4.1 Layout

Figures 36(A) and 36(B) show the Pro-Engineer models of the assembled right wing mounted on the back wing support plate that links the wing to the flyer. The left wing is a mirror image of the right wing. However, the mounting of the two wings on the support plate is different: the right wing sits on top of the left wing (see Figure 8(B)) in both stowed and deployed configurations.

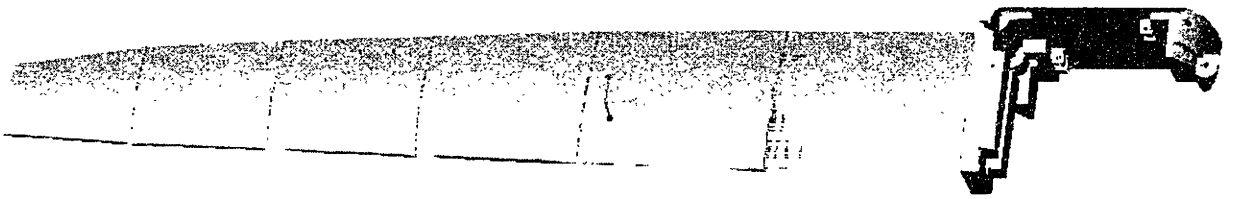

FIGURE 36(A): VIEW OF THE ASSEMBLED RIGHT WING: UPPER SURFACE

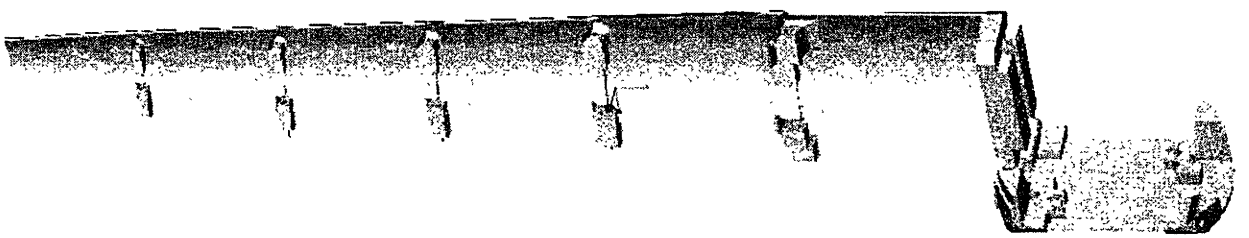

FIGURE 36(B): VIEW OF THE ASSEMBLED RIGHT WING: LOWER SURFACE

The following two Figures are pictures of the underside of the assembled left wing, showing the springs. The machined aluminum wing, that survived the high-g air gun tests, can be seen.

FIGURE 37(A): VIEW OF UNDERSIDE OF WING: SPRINGS AND HINGE PROTUBERANCES

FIGURE 37(B): VIEW OF UNDERSIDE OF WING: WING PANEL TAPER

The wing geometric characteristics are summarized in Table 6.

TABLE 6: WING GEOMETRIC CHARACTERISTICS

Wing Section	Area (m^2*10^{-3})	Root Chord (m)	Tip Chord (m)	Span (m)
1	6.581	0.0762	0.0762	0.0864
2	6.065	0.0762	0.0719	0.0825
3	4.946	0.0719	0.0652	0.0723
4	4.057	0.0652	0.0593	0.0653
5	3.365	0.0593	0.0532	0.0599
6	2.632	0.0532	0.0385	0.0575
TOTAL	27.646	-	-	0.423

Both wings together have a span of 0.846 m and 0.945 m (including the body), from wing tip to tip. Both wings together have an area of 0.0553 m^2. The wing mean average chord is 0.0647 m.

5.4.2 Deployment

Figure 38 illustrates the wing deployment sequence from stowed to deployed. From this Figure, it can be seen that the tip wing sections are folded into the root wing sections, that is, the smaller wing sections are contained in between the larger ones. Therefore, to deploy, wing section

2 describes a 180° arc from stowed position to deployed position, wing section 3 describes a 360° arc, wing section 4 a 540° arc, wing section 5 a 720° arc, wing section 6 a 900° arc.

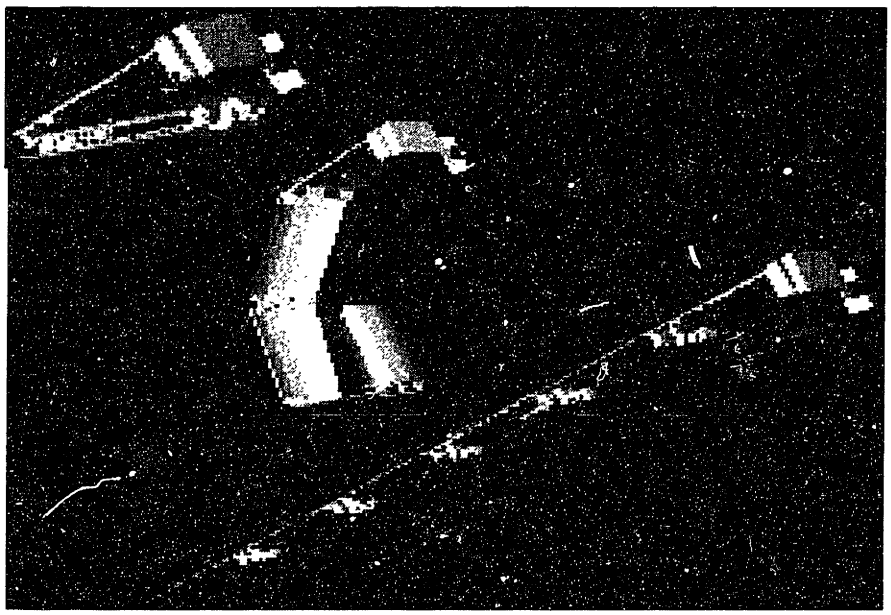

FIGURE 38: WING DEPLOYMENT

Chapter 6 Subsystems Integration

6.1 Modules Sub-Assemblies

The three flyer modules and their sub-assemblies are described in the following.

6.1.1 Propulsion Module

The propulsion module constitutes the forward cone section of the flyer. It includes the engine support plate, the engine itself, its high-g casing, the engine starting system, the servo motor for throttle control, the extended drive shaft and universal joint, and the yoke-folding propeller-cone sub-assembly (see Figure 39).

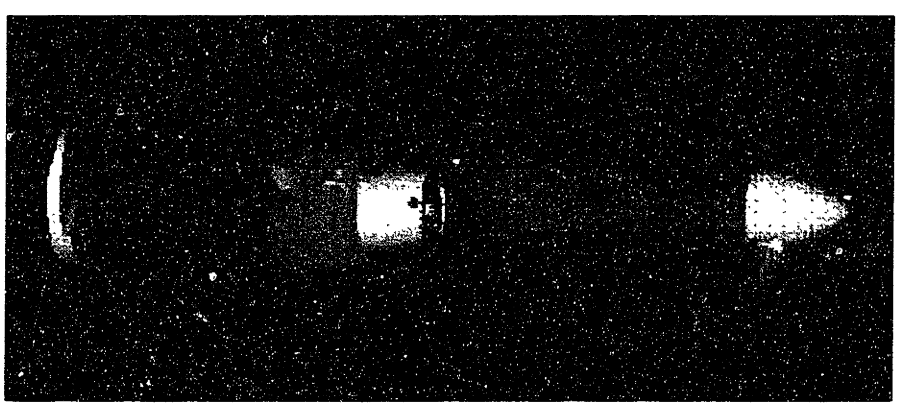

FIGURE 39: EXPLODED VIEW OF THE PROPULSION MODULE

The engine is an O.S. 15 FP engine developing 0.42 horsepower. Selection of this engine was the result of trying to incorporate the largest power output engine within the tight volume available. The propeller is a folding propeller with its blades sitting in cavities grooved in the cone.

6.1.2 Wing Module

The wing module includes the wings subsystem, the sensor, the fuel tank and the batteries. The two latter are located just behind the engine support plate. Batteries are wrapped around the fuel tank and embedded in a special high-g wax. A camera is located under the wings looking straight down at the ground.

The wing subsystem includes the right and the left 6-section-wings connected to the support plate which is connected to the wing module using four screws. Also included in the subsystem are the support blocks, and the cover plates covering half of each side of the wing cut out.

Figures 40 and 41 show views of the wing subsystem integrated in the wing module.

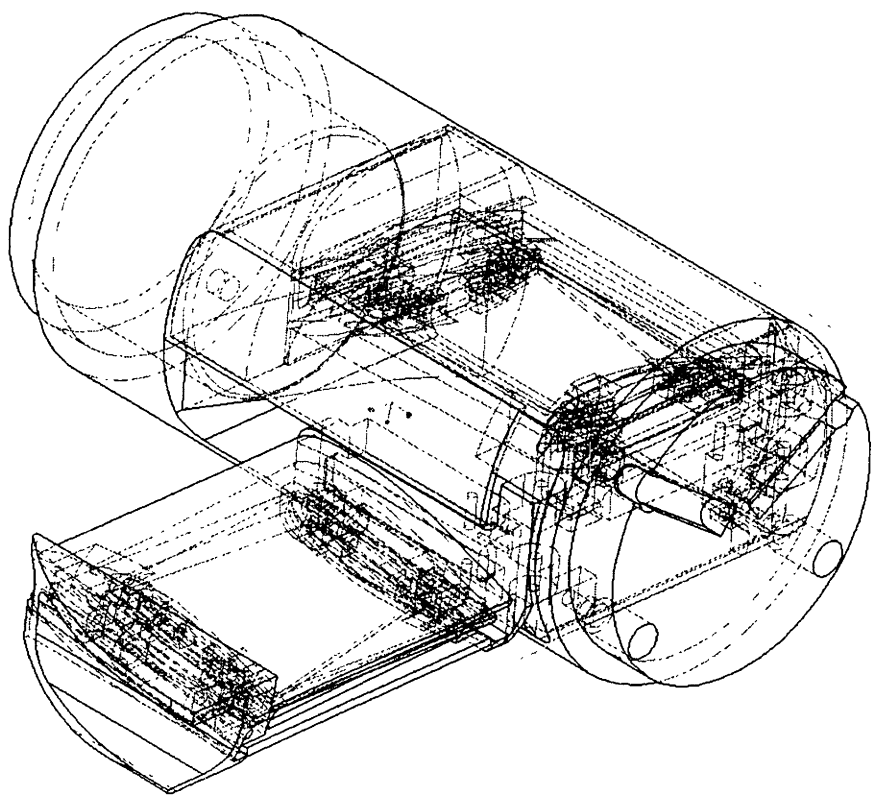

FIGURE 40: WIREFRAME OF WINGS AND WING MODULE

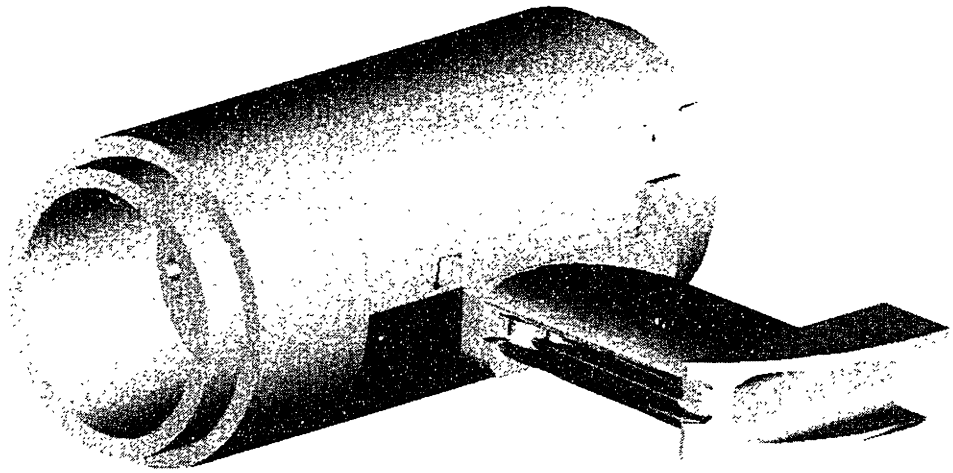

FIGURE 41: STOWED WING PIVOTED OUT OF WING MODULE

The following Figures show the machined aluminum wing module and the integrated left wing.

FIGURE 42: TOP VIEW OF WING AND WING MODULE

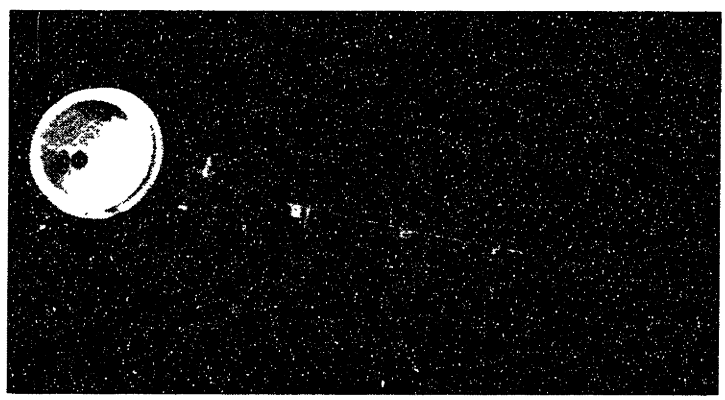

FIGURE 43: FRONT VIEW OF WING AND WING MODULE

6.1.3 Tail Module

The tail module (see Figure 44) includes the tails, their two servo motors, and all the necessary guidance, navigation and control equipment.

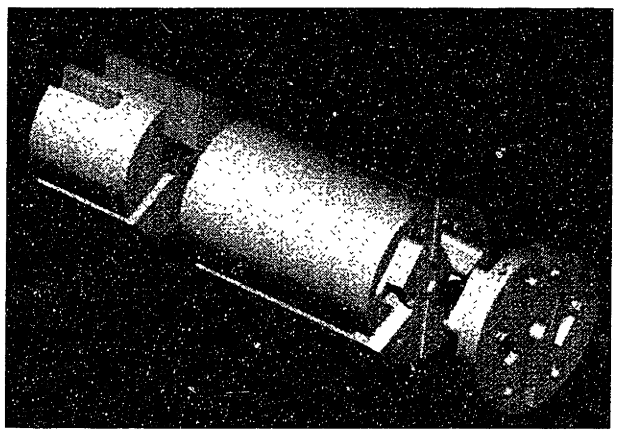

FIGURE 44: EXPLODED VIEW OF THE TAIL MODULE

The cuts through the tail module are the hosts for the two tails. Tails deploy out of the module by rotating 90^{o} about a pivot point located at the back of the module. Once this rotation is completed, a plus and minus 10^{o} pitch rotation is possible.

6.2 Shell / flyer Integration

Figure 45 shows the assembly of the shell and the back end. Six fins are attached on the back end and their role is to stabilize the shell during the ballistic phase and transition phase. The back end is also the host of the parachute that extracts the flyer from the shell. This one is empty on the Figure, and the void shows the space available to store the flyer. This shell is a modified illumination round that was machined at its base to accommodate a connector linking it to the back end. The interior of the shell was also machined, in the nose region, to accommodate the cone of the flyer.

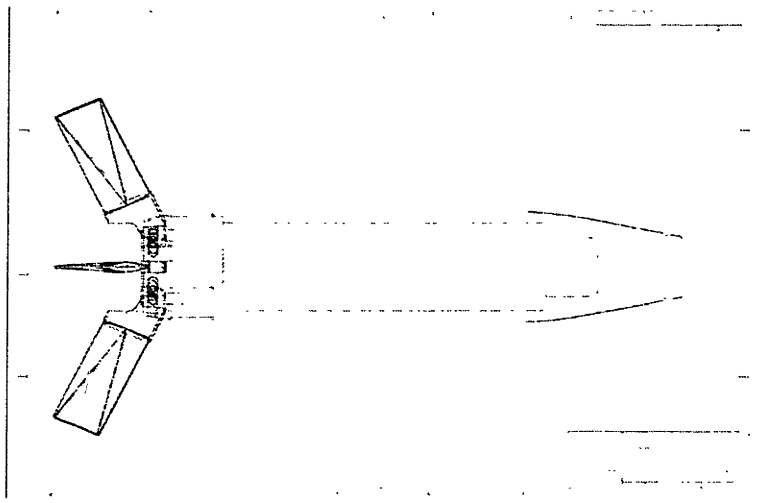

FIGURE 45: CROSS-SECTION OF SHELL-BACK-END ASSEMBLY

Figure 46 shows two cross section views of the flyer inserted in the shell-back-end assembly. This constitutes the whole Wide Area Surveillance Projectile system.

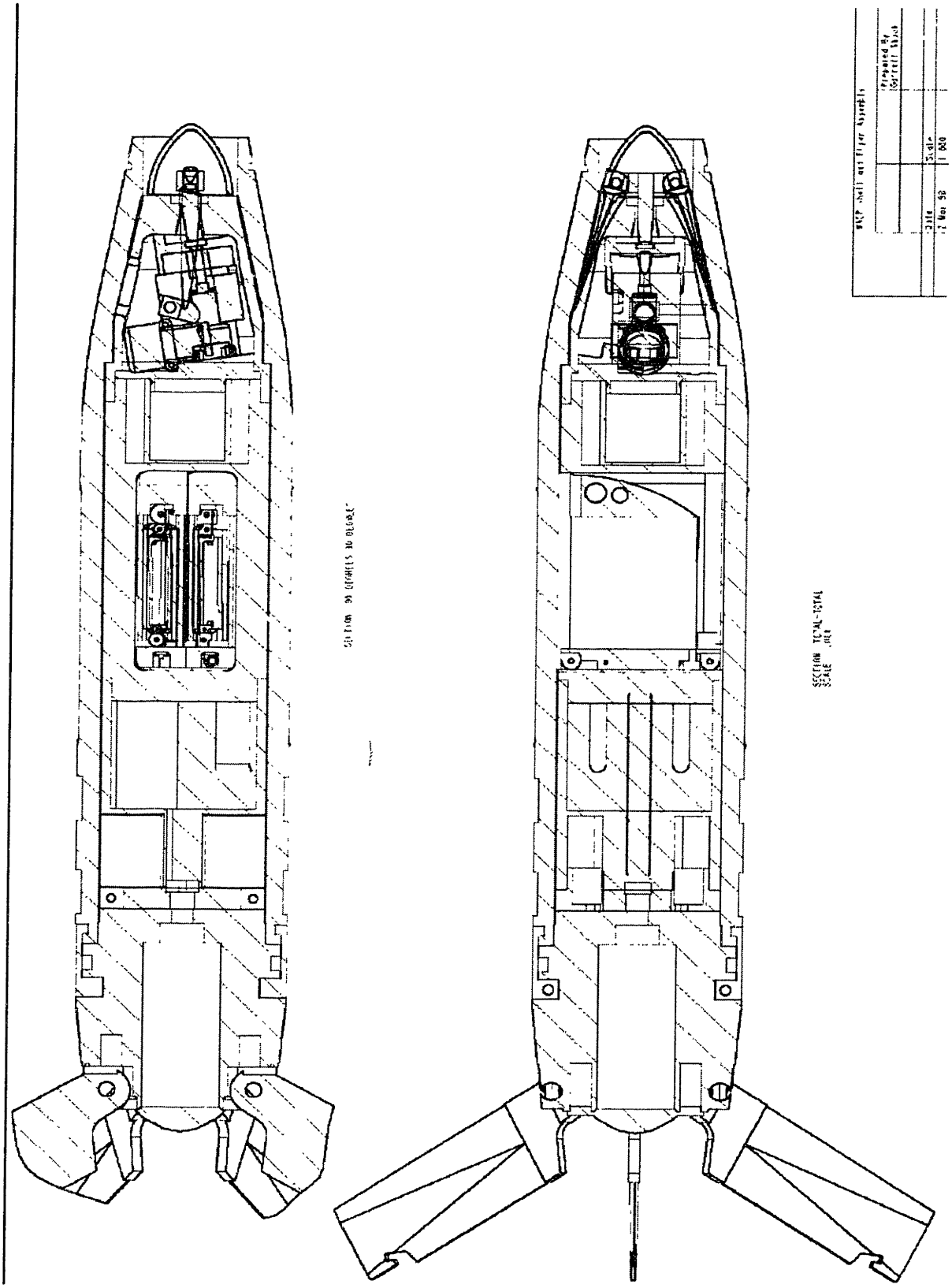

FIGURE 46: CROSS SECTIONS OF SHELL-FLYER INTEGRATION

6.3 Shell / Flyer Separation Mechanism

Figure 47 shows the Shell-back-end assembly, as it is during the ballistic phase.

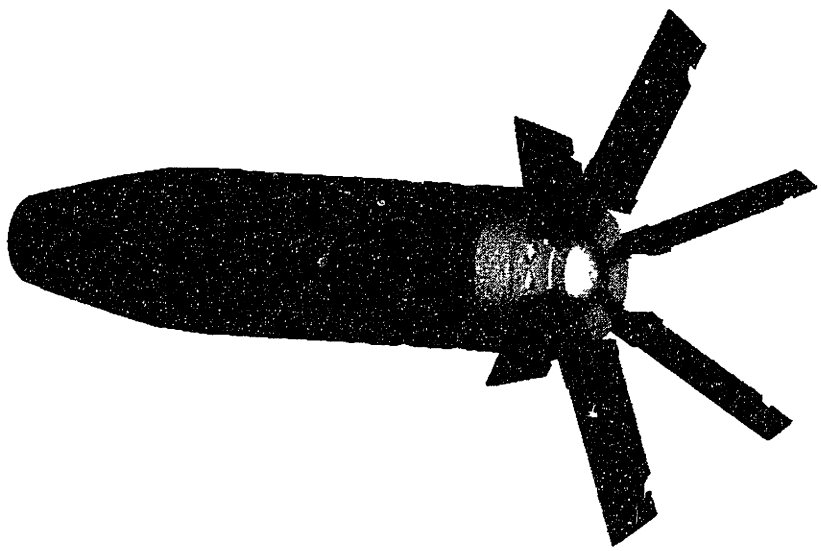

FIGURE 47: SHELL-BACK-END ASSEMBLY

At the end of the ballistic phase, the separation mechanism is initiated. Figure 48 shows the elements of the separation mechanism. The separation time sequence is as follows. First, the chute cover is ejected out of the back of the back-end using bolt thrusters, pulling the parachute with it and initiating parachute deployment. At the same time, the two clamps holding the shell and the back end ("base" on the Figure) together are cut through by a linear shape charge, thus freeing the shell from the back end. This back-end is connected to the flyer and the flyer-back-end assembly is pulled out of the shell by the parachute (see Figure 49). The shell then falls and the two flyer tails can deploy, as well as the propeller. At this moment also, the engine starts. A parachute deceleration period of twelve to fifteen seconds follows, so that the flyer-back-end assembly can slow down to a velocity of approximately 300 feet per second or 91 meters per second. Then the wings can safely deploy. Right after wing deployment the back-end-parachute assembly is separated from the flyer via the activation of an explosive bolt. The flyer is then free and can start its reconnaissance mission.

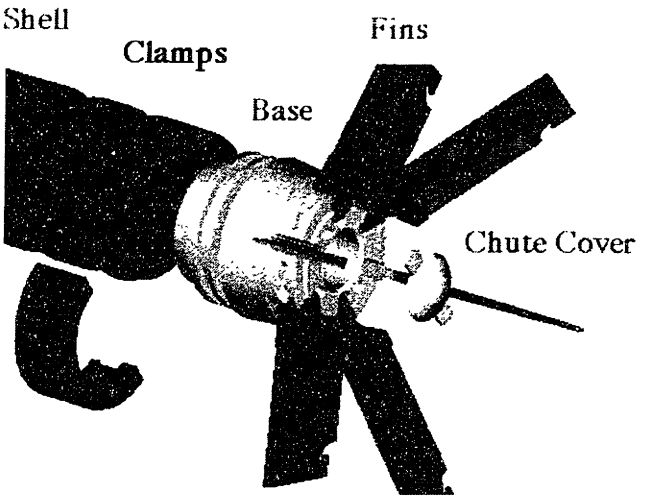

FIGURE 48: ELEMENTS OF SHELL-FLYER EXTRACTION

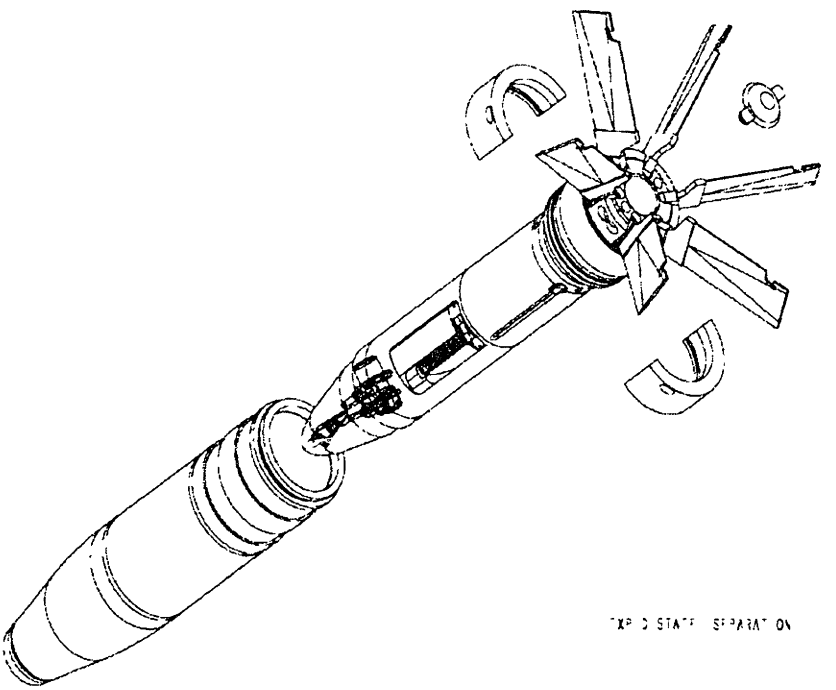

FIGURE 49: FLYER-SHELL EXTRACTION

6.4 Fully Deployed Flyer

Figures 50 and 51 show the pictures of the actual flyer and shell, with wings stowed and wings deployed, respectively. The shell as it appears in the picture was not quite in the "mission ready" state. In fact it was ready to be shipped to Dahlgren, the Navy Surface Warfare Test Center, were it was inserted in a canister and gun-tested, with the flyer inside on May 14 1998. The fins in the picture were not be used for this particular test due to length constraints.

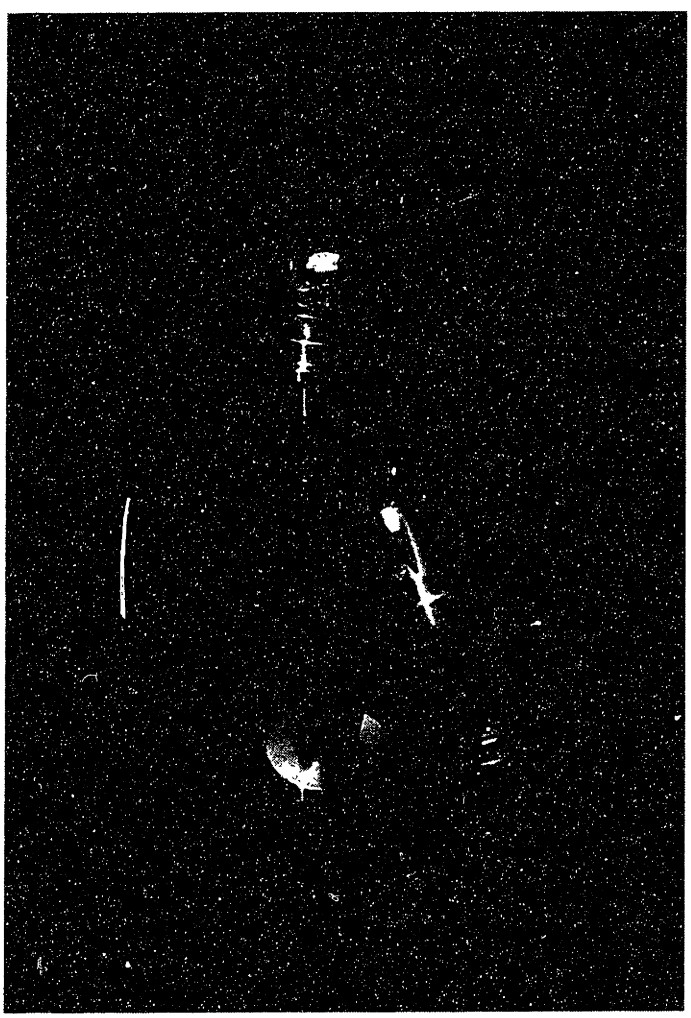

FIGURE 50: SHELL AND FLYER WITH WINGS STOWED

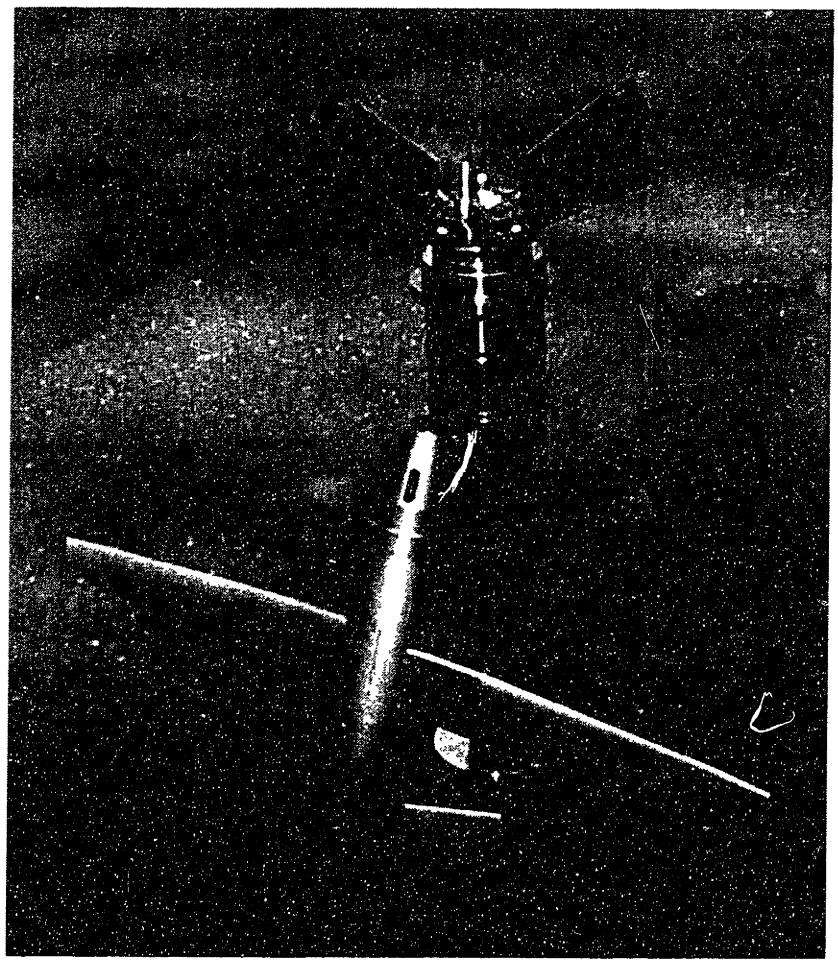

FIGURE 51: FULLY DEPLOYED FLYER WITH SHELL

Figure 52 shows a Pro-Engineer model of the final WASP flyer. This model has added features the actual flyer did not have at the time the picture was taken (Figures 50 and 51). These are the folding propeller, the nose cone, the wing cut out cover plates and the two small vertical fins.

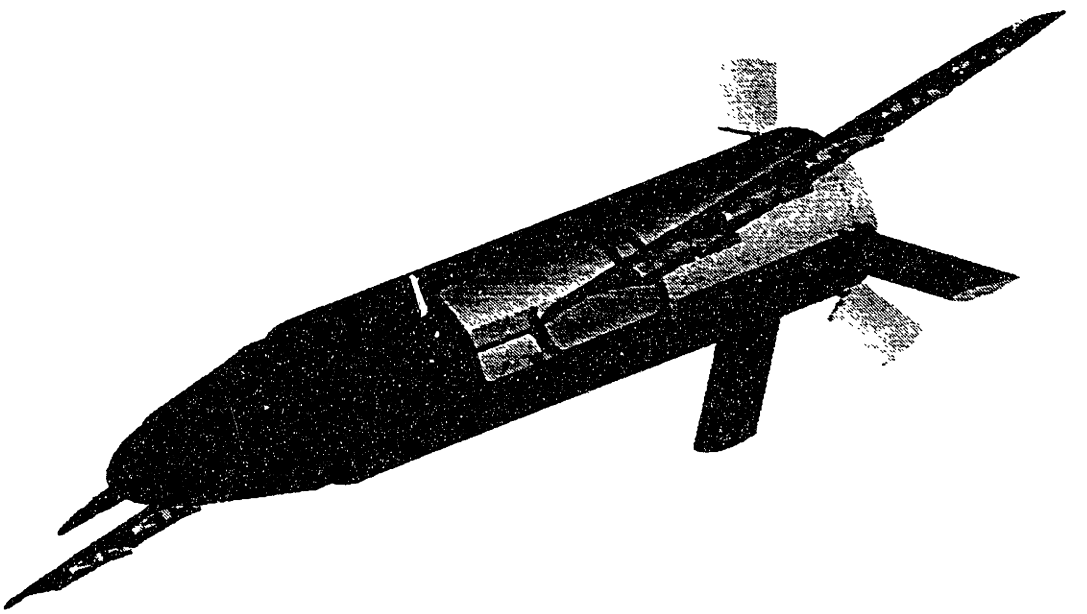

FIGURE 52: FINAL DEPLOYED FLYER PRO-ENGINEER MODEL

Chapter 7 Field Testing

The real gun test was performed on May 14th, 1998, at the Navy Surface Warfare Center, Dahlgren, Virginia. The main goal was to validate the structure and deployment mechanisms integrity of the High-g Vehicle in a real gun-launch environment. The Center did not allow the deployment of the vehicle because of the risk of landing in an inhabited region immediately surrounding it. A canister test was performed, enclosing the HGV in an 8-inch canister (Figure 53).

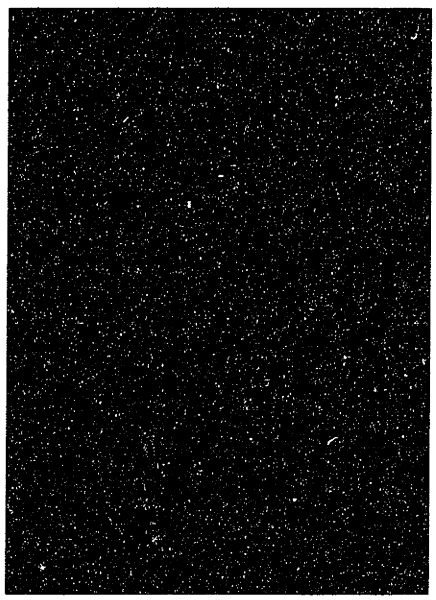

FIGURE 53: 8-INCH TEST CANISTER

For this test, the HGV was modified to fit in the canister. Attachment points were added at the nose and base of the test article and the fins were not mounted due to the constrained internal space of the 8-inch canister. Figure 54 shows the test article in preparation to be mounted in the canister.

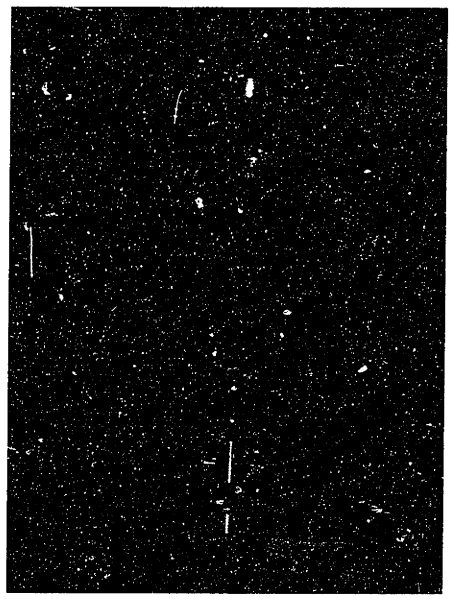

FIGURE 54: TEST ARTICLE WITH CANISTER FITTINGS

Then the test article-canister assembly was loaded into an 8-inch gun (Figure 55). The gun fired the canister at a 75^{o} elevation. The canister landed on water and was recovered. Figure 56 shows the canister after the recovery, in the disassembly room.

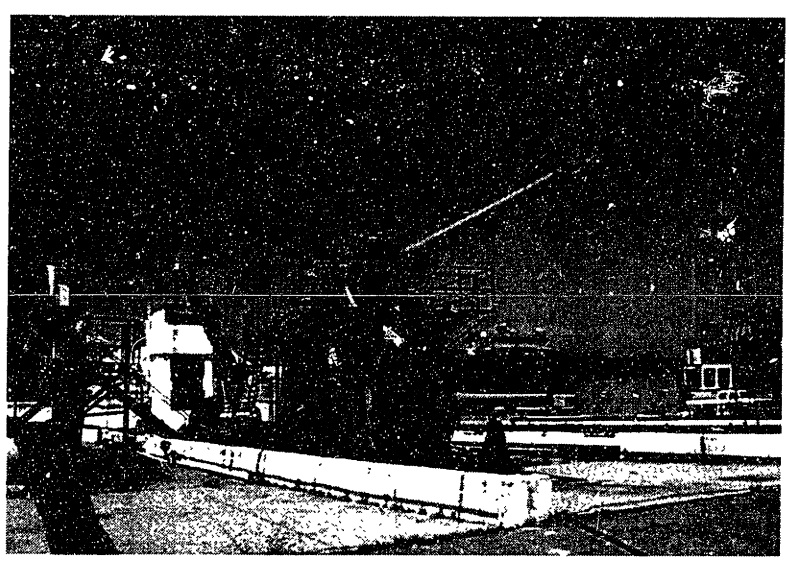

FIGURE 55: 8-INCH GUN

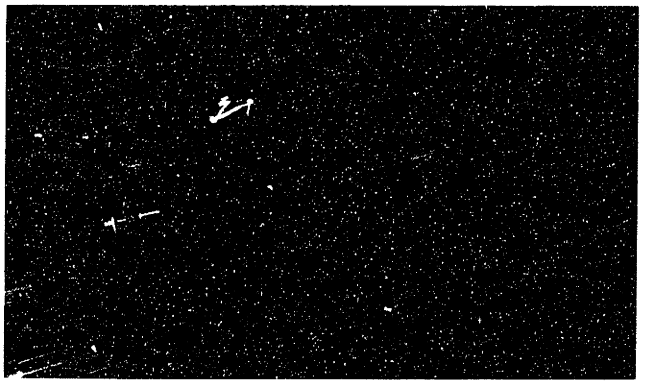

FIGURE 56: TEST CANISTER AFTER RECOVERY

A disassembly was then performed, removing first the HGV from the 8-inch canister. The HGV was set horizontally on a table and the flyer was pulled from the back with only very little force. Pulling it freed the tails first which deployed normally, showing no sign of stress from the gun launch. The flyer was completely pulled out of its shell, showing no sign of damage whatsoever. Figure 57 shows a close up of the stowed wings, with no sign of damage.

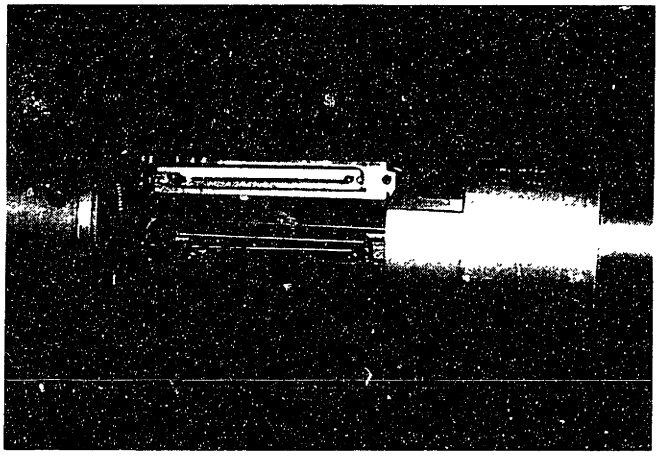

FIGURE 57: VIEW OF STOWED WINGS AFTER SHELL DISASSEMBLY

The wings were then deployed showing no damage and no added resistance compared to its condition before the gun launch. Figure 58 shows the wings fully deployed, with the flyer intact, as it appeared before the launch.

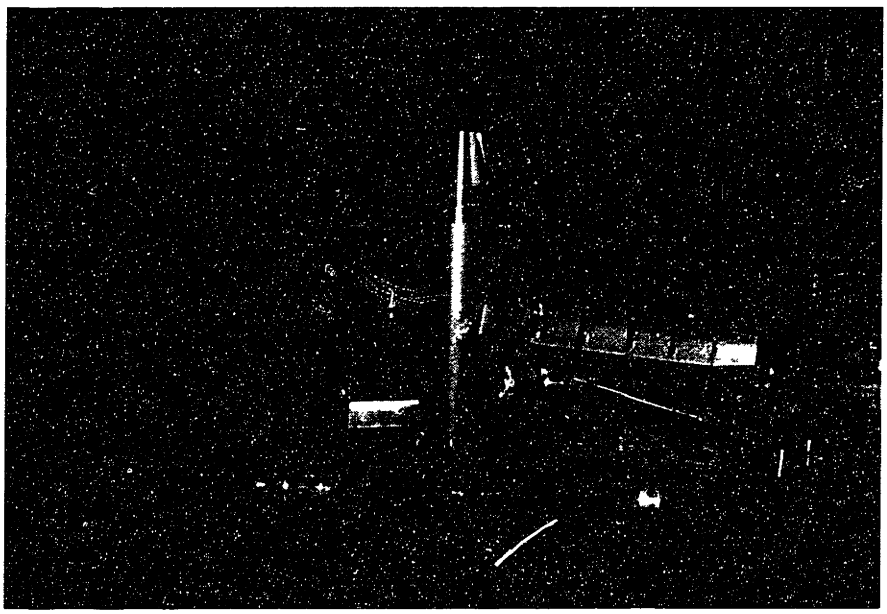

FIGURE 58: INTACT, FULLY DEPLOYED FLYER AFTER SHELL DISASSEMBLY

The May 14th Dahlgren test was a success, showing an intact flyer after a real gun launch of 12026 g's. Moreover, the Navy indicates that a successful 8-inch canister test ensures a 99% successful 5-inch operational vehicle gun launch.

Chapter 8 Conclusions

8.1 Achievements

8.1.1 Wing Design

The compact, high-g, high efficiency folding wing development spanned the second year of the MIT / Draper technology development partnership project, from June 1997 to June 1998. The wing development included a wing deployment concept, an aerodynamic analysis of the integrated wing-flyer system, wind tunnel testing, geometric structural analyses, the manufacturing of a prototype wing subsystem and its successful high-g survivability testing.

8.1.2 Total System Design

The Dahlgren testing proved that the High-g Vehicle along with its components could survive the high-g environment of a real gun fire. These components include the wings, the HGV structure, the tail surfaces and their actuators.

Still to be proven at this time are the aerodynamic characteristics and the sensor image quality of the Operational Vehicle. This will be demonstrated by the Flight Test Vehicle in the near future.

Furthermore, separate tests still have to be conducted to validate the shell-back-end separation, the back-end-flyer separation, and the parachute effectiveness.

8.2 Lessons Learned

Major unpredictables in the project were related to part manufacturing. Due to the team members' limited experience with manufacturing processes and design for manufacturing implementations, many part completion deadlines had to be pushed back in time. This problem became less apparent with time as valuable experience in the field was acquired, for example, through meetings with machinists at the design phase of a part.

A global vision of the status of a project is essential to determine its successful meeting of the deadlines. An efficient means of providing this vision is the use of a weekly updated schedule on which major events and deadlines are clearly visible. This exercise is especially helpful in defining the critical tasks leading to the most efficient task assignments to achieve the preset goals. The schedule exercise was not always well maintained by the team, perhaps due to its time consuming characteristics. However, in many instances the schedule clearly helped in defining critical tasks, in coordinating the efforts, and in meeting important deadlines such as field tests.

The team working environment was efficient due to the large design room including a desk for all team members, and all necessary computer tools. The team moved into this room early in the academic year from a much smaller room which couldn't comfortably accommodate all team members at the same time. The new room working environment very quickly saw an increase of efficiency of the team work, having team members working closer together, creating a better flow of information and a better global view and status of the whole project.

8.3 Project Spin-Offs

Throughout the project and especially towards the later stages of the high-g vehicle development, a growing outside interest in the system was noted. The reasons for this interest most certainly lie in the system being first-of-a kind and in the system showing growing signs of achieving its goals. One of the most interested parties was the Office of Naval Research (ONR) when the project was presented to some of its directors. The ONR was at the point of distributing a Small

Business-Innovative-Research (SBIR) fund to develop a vehicle that could have a range of at least 35 miles while carrying a payload and being gun-launched. The MIT vehicle created great interest and a request for a vehicle proposal to achieve these requirements was received. Figure 53 shows the "second" Wide Area Surveillance Projectile ("WASP 2"), a possible configuration of the new vehicle. It is an extended version (36-inch body length) of the actual vehicle with more space for fuel and payload.

The feasibility of a compact, high-g, high efficiency wing system created a growing interest of its own, being one of the major design challenges of a gun-launched aircraft. The Forward Air Support-Marine (FASM) program, a long-range cannon launched vehicle to be developed by SAIC, was in its preliminary design phase and asked the MIT / Draper team for a high-g folding wing proposal, as a fall-back plan for an inflatable wing system. A short preliminary study was then conducted, based on the FASM predicted weight, cruise conditions and geometry, and a proposal was prepared.

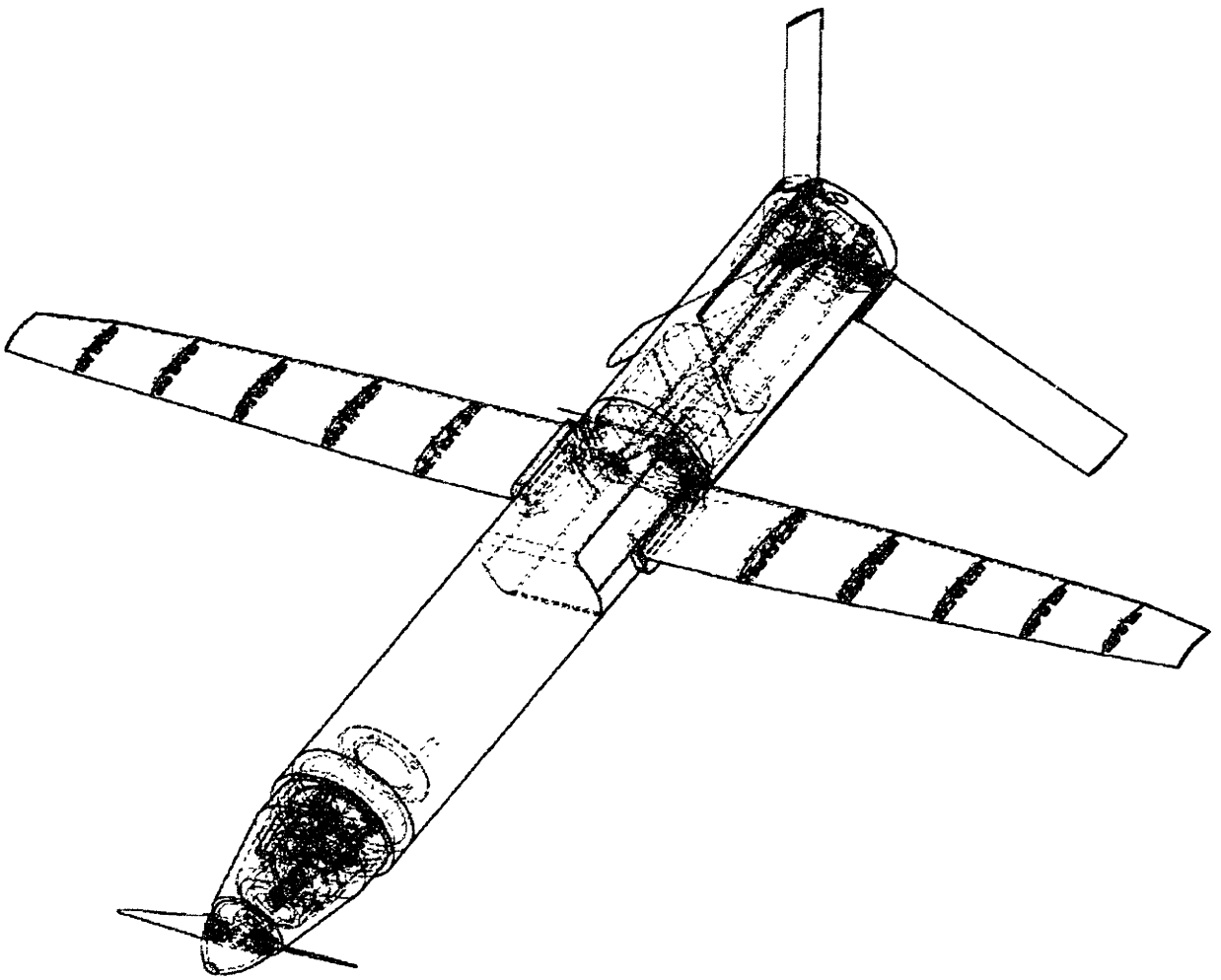

FIGURE 59: "WASP 2"

References

1.- Jane's All the World Aircraft 1959-60, p.303

2.- Bovais, C.S., Haupt, M.E. & Toot, P.L., Flight Testing with Sub-Scale Remotely Piloted Drop Models, Washington D.C., 1992, AIAA 92-4079

3.- Drela, Mark, Class Notes for 16.110 Flight Vehicles Aerodynamics, MIT, 1997-98

4.- Iranzo-Greus, David, Rapid-Response Surveillance System Design and Aerodynamic Modeling, Cambridge MA, 1997.

5.- Katch, Sebastien, Concept Development, Mechanical Design, Manufacturing and Experimental Testing for a Canon Launched Reconnaissance Vehicle, Cambridge MA, 1998.

6.- Gavrilets, Vladislav, Avionics Systems Development for Small Unmanned Aircraft, Cambridge MA, 1998.

7.- Airset, a geometry manipulation program supplied by M. Drela.

8.- Gerard, George & Becker, Herbert, Buckling of Curved plates and Shells, Washington D.C., 1957, NACA TN 3783

9.- Shigley & Mischke, Mechanical Engineering Design

10.- Chiu, Rodney, Wide Area Surveillance Projectile Deployment Sequence, Cambridge MA, 1998.

11.- Shook, Garrett, Design, Assembly and Test of a Launch and Flight Support and Deployment System for a Gun-Launch Reconnaissance Vehicle, Cambridge MA, 1998.

12.- Hauss, Jean-Marc, Design of an Unmanned Aerial Vehicle, Cambridge MA, 1998.

Appendix A Typical Project Schedule

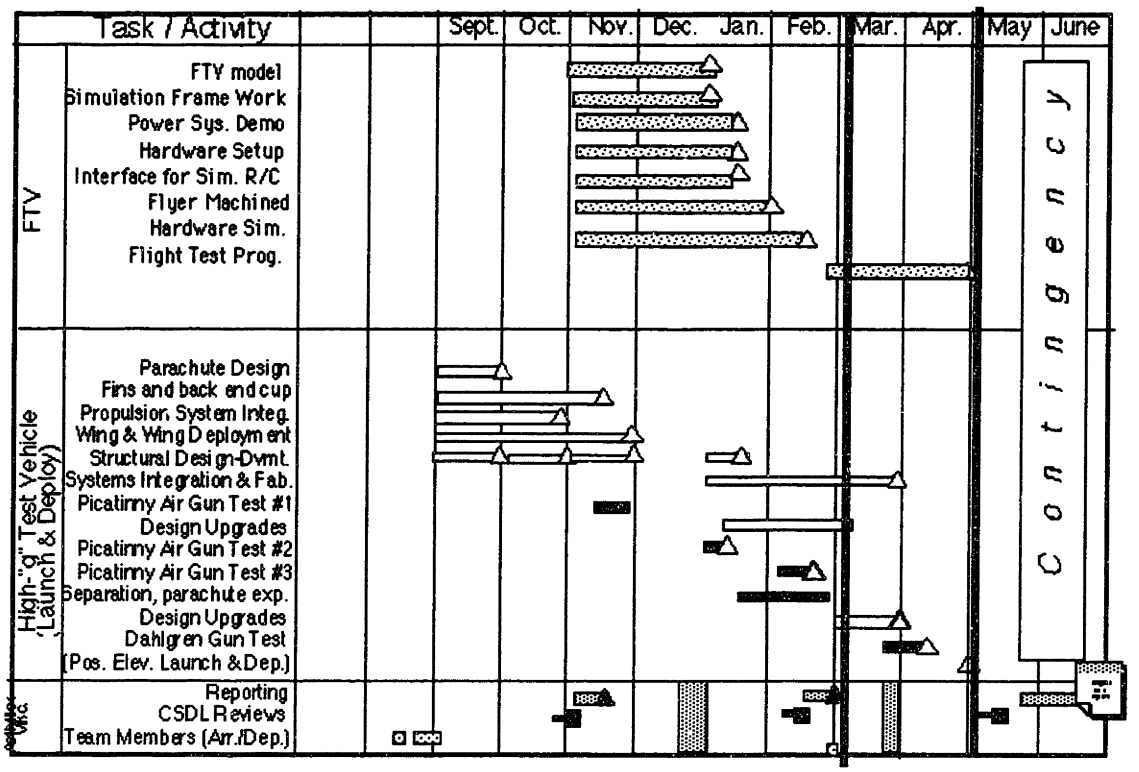

Appendix B Information on Inflatable Wings

PRIMEX
AEROSPACE COMPANY

July 21, 1997
Ref. No. 10350-97-053

Mr. Thierry Lasiez
Massachusetts Institute of Technology
77 Massachusetts Avenue
Room 33-212
Cambridge, Massachusetts 02139

Dear Thierry:

Enclosed is some information on the inflatable tube spar wing developed by Vertigo. Please feel free to call them directly.

I have also enclosed a piece of a "drop-stitch" airfoil. The tape on the ends approximates the leading and tracking edge closures. These closures would normally be fabricated from fabric similar to the wing skin and bonded into place.

As we discussed, Primex Aerospace has the experience and capability to provide the entire wing and inflation system as a package.

If you have any questions, please contact me @ (425) 882-5772.

Sincerely,

Randel L. Hoskins, P.E.
Director, Advanced Development

RLH/ym217

Enclosure

PRIMEX AEROSPACE COMPANY
A Wholly Owned Subsidiary of PRIMEX Technologies, Inc.
P.O. Box 97009 • 11441 Willows Road N.E., Redmond, WA 98073-9709 • Telephone (206) 885-5000 • Fax (206) 882-5804

FIGURE B1: INFLATABLE WING PROPOSAL

VERTIGO INC.

AERONAUTICAL ENGINEERING AND DEVELOPMENT

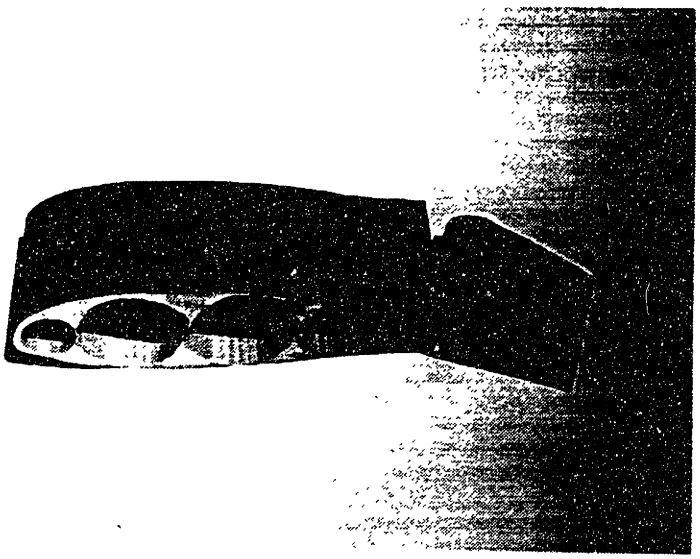

Inflatable Wing

- Stows in small volume
- Deploys rapidly
- High strength for cantilever configurations
- Impact damage resistant
- Inflatable control surface and actuating torque tube.
- High pressure braided Kevlar spars.*
- Ram pressure in open cell foam supports skin.*

*Patents Pending

PO BOX 117 • LAKE ELSINORE, CA 92531-0117 • (909) 674-0604 • FAX (909) 674-5461

FIGURE B2: INFLATABLE WING DESIGN

Appendix C Gun Tests and Gun Environments

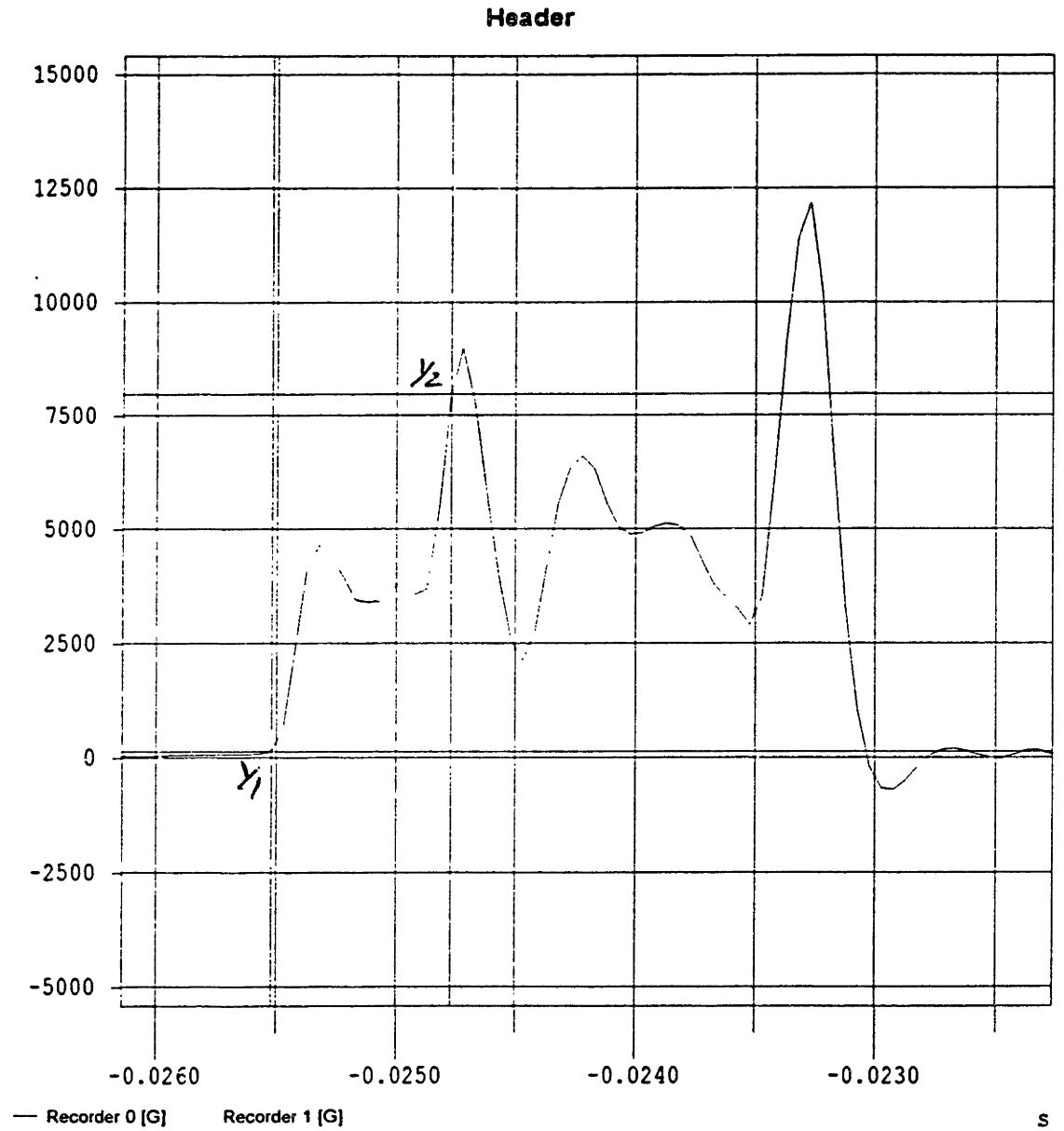

Channel:Recorder 0

Y1:	130.114944 G	Y2:	7964.489746 G
t1:	-0.0255 s	t2:	-0.0248 s
dt:	0.00075 s	f:	1333.333333 Hz
dY:	7834.374802	dY/dt:	10.446E06
Min:	130.114944	Max:	7964.489746
Int:	2.744195	RMS:	4062.571205

FIGURE C1: SAMPLE TEST OF AIR GUN

EXAMPLES - HIGH "G" PROFILES

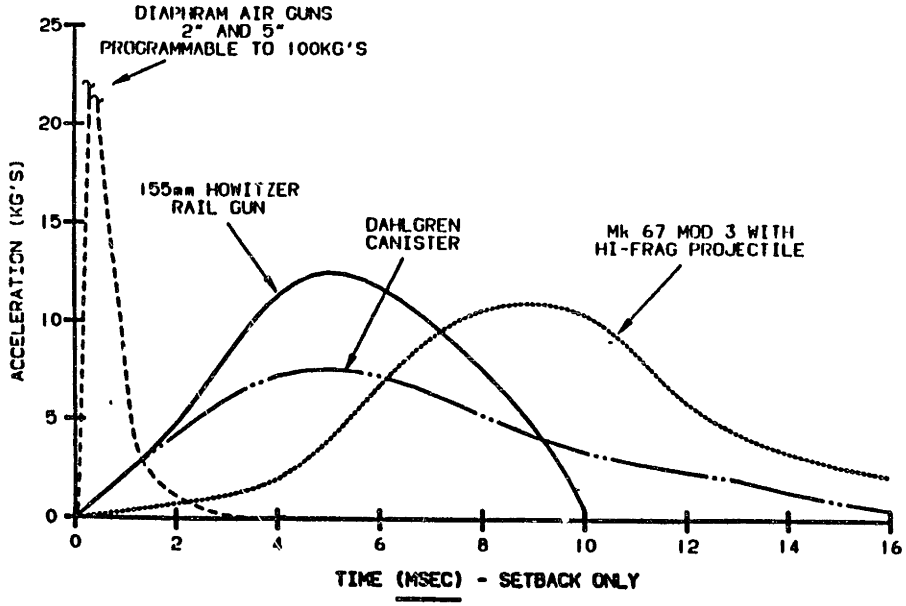

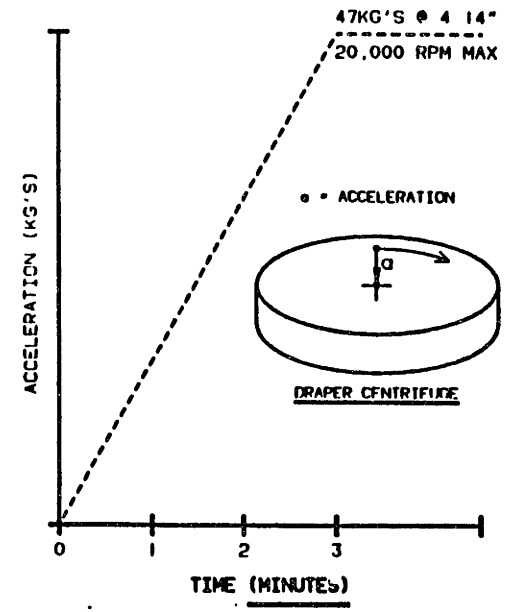

FIGURE C2: GUN ENVIRONMENTS

DRAPER LABORATORY
F PETKUNAS 10-97

Appendix D Software Input Codes

AVL flyer Definition code

```
Illuminating Round Flyer
!Mach
0.115
!IYsym  IZsym  Zsym
0       0      0.0
!Sref   Cref   Bref
553     6.47   945
!Xref   Yref   Zref
-20.8   0.0    0
!
SURFACE
Main Wing Right
!Nchordwise  Cspace
6            3.0
HINGE
0.0 1.0 0.0
YDUPLICATE
0.0
SECTION
!Xle   Yle   Zle   Chord   Ainc  Nspanwise  Sspace
-22.72 5     0     7.62    0     8          1.0
AFILE
t16thick23
SECTION
!Xle   Yle   Zle   Chord   Ainc  Nspanwise  Sspace
-21.6  47.3  5     5.39    0     8          1.0
AFILE
t16thick23
!
SURFACE
FuselageH
!Nchordwise  Cspace
8            1.0
YDUPLICATE
 0.0
SECTION
!Xle   Yle   Zle   Chord   Ainc  Nspanwise  Sspace
-52    0     0     52      0.    4          1.0
```

```
SECTION
!Xle   Yle   Zle    Chord   Ainc  Nspanwise  Sspace
-52    0.75  0.     52      0.    4          1.0
SECTION
!Xle   Yle   Zle    Chord   Ainc  Nspanwise  Sspace
-33    5     0.     33      0.    4          1.0
!
SURFACE
FuselageV
!Nchordwise  Cspace
8            1.0
SECTION
!Xle   Yle   Zle    Chord   Ainc  Nspanwise  Sspace
-33    0     -5     33      0.    4          1.0
SECTION
!Xle   Yle   Zle    Chord   Ainc  Nspanwise  Sspace
-52    0     -0.75  52      0.    4          1.0
SECTION
!Xle   Yle   Zle    Chord   Ainc  Nspanwise  Sspace
-52    0     0      52      0.    4          1.0
SECTION
!Xle   Yle   Zle    Chord   Ainc  Nspanwise  Sspace
-52    0     0.75   52      0.    4          1.0
SECTION
!Xle   Yle   Zle    Chord   Ainc  Nspanwise  Sspace
-33    0     5      33      0.    4          1.0
!
SURFACE
Tail
!Nchordwise  Cspace
4            1.0
YDUPLICATE
0.0
HINGE
0.0 1.0 -0.7
SECTION
!Xle   Yle   Zle    Chord   Ainc  Nspanwise  Sspace
-4.4   4.10  -2.87  4.4     0.    6          1.0
AFILE
naca2413rev
SECTION
!Xle   Yle   Zle    Chord   Ainc  Nspanwise  Sspace
-4.4   13.52 -9.47  4.4     0.    6          1.0
AFILE
naca2413rev
!
```

```
SURFACE
VerticalStabTop
!Nchordwise  Cspace
4          1.0
SECTION
!Xle   Yle   Zle    Chord   Ainc  Nspanwise  Sspace
-3.8   0     5      3.8     0.    6          1.0
AFILE
naca009
SECTION
!Xle   Yle   Zle    Chord   Ainc  Nspanwise  Sspace
-1.03  0     10.54  3.8     0.    6          1.0
AFILE
naca009
!
SURFACE
VerticalStabBottom
!Nchordwise  Cspace
4          1.0
SECTION
!Xle   Yle   Zle    Chord   Ainc  Nspanwise  Sspace
-3.8   0     -5     3.8     0.    6          1.0
AFILE
naca009
SECTION
!Xle   Yle   Zle    Chord   Ainc  Nspanwise  Sspace
-1.03  0     -10.54 3.8     0.    6          1.0
AFILE
naca009
!
```

Matlab spring analysis ".m"file

```
% Program to calculate the Torque of torsion springs
clear;

for i = 1:1:50

d(i) = 0.045+i*0.0005;
axialspace = 1;

od = 0.5;
```

```
D(i) = od - d(i);
C(i) = D / d;
Ki(i) = (4*C(i)^2-C(i)-1)/(4*C(i)*(C(i)-1));
sigma = 275000;
N(i) = (axialspace ./ d(i)) - 2;
E = 27.6e6;

teta(i) = pi.*sigma.*2.*D(i).*N(i) ./ (Ki(i).*d(i).*E);
Torque(i) = (teta(i)-pi).*E.*(d(i).^4)./(64.*D(i).*N(i));

i=i+1;

end

plot(d,Torque);
xlabel('Wire Diameter [in]');
ylabel('Torque [in.lb]');
grid

TETA = teta*180/pi
d
```

Wing Airfoil coordinates: modified T16 airfoil

```
_T 16
  1.002940 0.012528
  0.994192 0.014565
  0.981260 0.017559
  0.964322 0.021457
  0.945494 0.025765
  0.926175 0.030154
  0.906782 0.034521
  0.887378 0.038837
  0.867983 0.043098
  0.848627 0.047285
  0.829303 0.051379
  0.810000 0.055369
  0.790707 0.059248
  0.771417 0.063007
  0.752124 0.066642
  0.732824 0.070148
  0.713515 0.073520
  0.694197 0.076754
  0.674869 0.079846
  0.655535 0.082792
  0.636197 0.085586
  0.616854 0.088222
  0.597509 0.090693
  0.578164 0.092995
  0.558819 0.095121
  0.539476 0.097064
  0.520137 0.098818
  0.500806 0.100377
  0.481483 0.101733
  0.462172 0.102878
  0.442879 0.103805
  0.423605 0.104505
```

0.404356 0.104970
0.385138 0.105190
0.365955 0.105155
0.346814 0.104854
0.327725 0.104279
0.308693 0.103414
0.289731 0.102249
0.270847 0.100770
0.252058 0.098962
0.233377 0.096809
0.214818 0.094296
0.196407 0.091407
0.178185 0.088125
0.160190 0.084425
0.142465 0.080282
0.125063 0.075670
0.108054 0.070566
0.091535 0.064948
0.075638 0.058806
0.060561 0.052159
0.046605 0.045086
0.034213 0.037803
0.023890 0.030697
0.015904 0.024201
0.010076 0.018540
0.005955 0.013686
0.003109 0.009479
0.001245 0.005756
0.000230 0.002388
0.000000 0.000000
0.000228 -0.002388
0.001797 -0.005515
0.004939 -0.007261
0.010610 -0.007266
0.017697 -0.005980
0.025064 -0.004242
0.033766 -0.002010
0.044624 0.000836
0.057778 0.004278
0.072485 0.008092
0.088276 0.012154
0.104769 0.016360
0.121666 0.020610
0.138752 0.024820
0.155946 0.028936
0.173232 0.032922
0.190611 0.036751
0.208092 0.040402
0.225681 0.043871
0.243379 0.047172
0.261209 0.050284
0.279201 0.053204
0.297356 0.055921
0.315658 0.058416
0.334093 0.060671
0.352644 0.062671
0.371300 0.064397
0.390042 0.065833
0.408856 0.066964
0.427728 0.067772
0.446646 0.068243
0.465595 0.068361
0.484565 0.068116
0.503545 0.067515
0.522527 0.066580
0.541507 0.065333
0.560485 0.063793
0.579455 0.061984
0.598416 0.059927
0.617364 0.057642
0.636296 0.055153
0.655207 0.052476
0.674097 0.049625
0.692973 0.046607
0.711835 0.043437
0.730691 0.040121
0.749553 0 036670
0.768433 0.033094
0.787340 0.029399
0.806289 0.025596
0.825288 0.021692

0.844251 0.017717
0.863370 0.013640
0.882527 0.009488
0.901640 0.005275
0.920644 0.001020
0.939472 -0.003263
0.957803 -0.007498
0 974420 -0.011390
0 987333 -0.014451
0.996067 -0.016540

Tail Airfoil Coordinates: Naca 2413 up side down

NACA 2413
1.000000 -0.001365
0.992632 -0.002968
0.979767 -0.005729
0.964764 -0.008887
0.948006 -0.012339
0.930053 -0.015949
0.911400 -0.019606
0.892370 -0.023240
0.873143 -0.026813
0.853811 -0.030309
0.834419 -0.033717
0.814990 -0.037035
0.795535 -0.040260
0 776061 -0 043392
0.756573 -0.046429
0 737075 -0.049370
0.717569 -0.052215
0.698059 -0.054961
0 678547 -0.057608
0.659036 -0.060153
0.639528 -0.062594
0.620028 -0.064929
0.600537 -0.067154
0.581059 -0.069268
0.561597 -0.071266
0 542155 -0.073145
0.522737 -0.074901
0.503348 -0.076528
0.483992 -0.078024
0.464677 -0.079381
0.445414 -0.080595
0.426221 -0.081659
0.407128 -0.082567
0.388203 -0.083301
0.369435 -0.083822
0.350772 -0.084123
0.332206 -0.084199
0.313735 -0.084042
0.295367 -0.083645
0.277113 -0.083000
0.258987 -0.082099
0.241008 -0.080933
0.223201 -0.079492
0.205594 -0.077770
0.188228 -0.075758
0.171153 -0.073451
0.154442 -0.070847
0.138191 -0.067954
0.122530 -0.064788
0.107625 -0.061385
0.093665 -0.057803
0.080842 -0.054118
0.069297 -0.050419
0.059092 -0.046785
0.050193 -0.043277
0.042494 -0.039927
0.035854 -0.036745
0.030122 -0.033723
0.025161 -0.030846
0.020853 -0.028094
0.017102 -0.025445

0.013831 -0.022879
0.010981 -0.020380
0.008508 -0.017929
0.006378 -0 015514
0.004572 -0.013124
0.003074 -0.010752
0.001879 -0.008398
0.000983 -0.006067
0.000379 -0.003762
0.000062 -0.001522
0.000012 0.000651
0.000224 0.002847
0.000735 0.005098
0.001566 0.007352
0.002727 0.009581
0.004220 0.011767
0.006041 0.013896
0.008190 0.015968
0.010675 0.017986
0 013514 0 019958
0.016736 0 021894
0.020386 0.023805
0.024525 0.025702
0.029233 0 027595
0.034614 0.029492
0.040795 0.031398
0.047933 0.033315
0.056204 0.035233
0.065784 0.037135
0.076818 0.038985
0.089366 0.040736
0.103373 0.042335
0.118672 0.043732
0.135030 0 044898
0.152213 0.045822
0.170020 0.046508
0.188302 0.046971
0.206948 0.047230
0.225882 0.047307
0.245050 0.047222
0.264412 0.046993
0.283938 0.046639
0.303606 0.046177
0.323395 0 045621
0.343288 0.044985
0.363262 0.044283
0.383287 0.043528
0.403302 0.042732
0.423246 0.041871
0.443188 0.040933
0.463156 0 039925
0.483161 0.038853
0.503206 0.037723
0.523289 0.036541
0.543410 0.035313
0.563563 0.034042
0.583747 0.032735
0.603958 0.031394
0.624194 0.030024
0.644450 0.028627
0.664724 0.027208
0.685013 0.025768
0.705315 0.024309
0.725626 0.022833
0.745943 0.021342
0.766264 0 019836
0.786584 0.018317
0.806900 0.016784
0.827204 0.015238
0.847485 0 013680
0.867719 0.012111
0.887859 0.010532
0.907807 0.008952
0.927364 0.007384
0.946170 0.005857
0.963666 0.004418
0.979230 0.003121
0.992469 0.002006
1.000000 0.001365

THESIS PROCESSING SLIP

FIXED FIELD: ill. _____ name _____

index _____ biblio _____

▶ COPIES: (Archives) (Aero) Dewey Eng Hum

Lindgren Music Rotch Science

TITLE VARIES: ▶☐ _____

NAME VARIES: ▶☑ Dominique _____

IMPRINT: (COPYRIGHT) _____

▶ COLLATION: 104p _____

▶ ADD. DEGREE: _____ ▶ DEPT.: _____

SUPERVISORS: _____

NOTES:

cat'r: date:

page: J154

▶ DEPT: Aero

▶ YEAR: 1998 ▶ DEGREE: M.Eng

▶ NAME: CASIEZ, Thierry D.